UCLouvain

epl

École polytechnique de Louvain

Design and experimental performance assessment of a hip flexion assistive device

Author: **Philippine de Suraÿ**
Supervisors: **Benoît Herman, Renaud Ronsse**
Readers: **Philippe Lefèvre, Virginie Otlet**
Academic year 2022–2023
Master [120] in Biomedical Engineering

Abstract

The aftermaths of stroke frequently result in hemiparesis among the survivors, inducing gait irregularities and hindering mobility. As the world witnesses an aging population, this disorder represents a pressing challenge with elderly being more prone to suffer from cerebrovascular diseases, including stroke.

In this context, wearable robotics emerge as a promising mean for restoring locomotion and improving the overall quality of life for stroke survivors. By providing functional support and addressing walking abnormalities, these technologies facilitates their rehabilitation efforts and empower them to regain independence. Lower-limb orthoses play an important role in enhancing balance and mobility for hemiparetic patients with the ultimate goal of restoring gait symmetry.

This study takes place in the creation of an active hip orthosis, H.E.R.O. - Hip Empowering Robotic Orthosis. This device aims at providing hip flexion assistance for people experiencing hemiparesis. The core focus of this work revolves around designing a control system able to synchronize with a patient's gait dynamics, while delivering a customizable and periodic assistive force. The challenge of dynamic adaptation to pace modifications is addressed with the implementation of a pool of adaptive oscillators.

Other considerations of this work include electro-mechanical and ergonomic enhancements. Issues had to be addressed regarding current saturation and the seamless integration of a parallel spring to ensure to exploit full motor capacity. As the human-robot interactions represent one of the main stakes of the project, this study emphasized the user's comfort while ensuring a safe use.

The H.E.R.O. prototype designed in this project holds great potential for assisting hemiparetic patients' gait and improving their autonomy. The performances achieved met the goals established. The device is now ready to enter the next phase of its development with the integration of a system able to detect the user's intentions.

Acknowledgements

I wish to extend my gratitude to all of who helped me accomplish this work. Their invaluable contribution by their guidance and support allowed me to carry out significant enhancements of the project and deliver this master's thesis.

- Special thanks to my supervisors, **Prof. Renaud Ronsse** and **Benoît Herman**. Without their insightful feedbacks and advises, this work would not have been possible. I am also grateful for their time, and the numerous hours spent in the lab, testing the prototype with me.
- Thanks to **Henri Laloyaux** for sharing with me his knowledge and work about adaptive oscillators and controllers. His contributions saved me from long hours implementing fastidious formulas.
- I would like to express my sincere gratitude to **Simon De Jaeger** for his dedication in helping me enhance the orthosis structure and for constantly encouraging me in my work.
- A warm thank you to **Thierry Darras** for providing me with adequate equipment and his understanding of electronics.
- Thank you to **Victor Lhoest** for his expertise in LabVIEW and his advice regarding the electronics.
- My appreciation extends to **Martin**, **Naomie**, **Camille**, **Julien** and **Nicolas** for their work of quality regarding this project.
- I am grateful for the research team of the office who taught me a lot.
- Lastly, I would like to thank my family and friends who helped me get there by supporting me during all these months, in the good and bad times.

Contents

Chapter 1

Introduction

1.1 Context

Stroke accounts for 7% of all deaths in Belgium, with around 15 000 new cases in 2019 [1]. Worldwide, stroke represents the second leading death cause [2] and its burden remains significant for the survivors. It is estimated that 75% of them will experience walking impairments, with varying degrees of severity [3].

Florent Moissenet from the *Centre National de Rééducation Fonctionelle et de Réadaptation - Rehazenter (Luxembourg)* expressed the will of the development of a device allowing to restore gait symmetry for hemiparetic patients by providing hip flexion assistance. This is where this work takes its essence with hemiparesis being the most common neurological disorder following a stroke [3]. The project was first launched by the master's thesis of Guillaumie and Lejeune back in 2017, under the supervision of Prof. Renaud Ronsse and Benoît Herman.

The clinical definition of a stroke is a neurologic deficit occurring when there is a disturbance in blood flow in a region of the brain. Approximately 80% of them are ischemic strokes caused by the obstruction of a blood vessel, whereas the remaining 20% are hemorrhagic strokes due to bleeding from a ruptured vessel wall [4, 5]. Hemiparesis is a partial weakness on one side of the body resulting from damage at the brain or spinal cord levels. The patients express mobility and balance abnormalities due to impairments in physiological systems like sensory feedback, cognitive processing, muscle control or motor planning [6].

Rehabilitation robotics for patients who suffered a stroke have proven their efficacy by offering a functional support assisting the walk of the patients. The use of lower-limb orthoses allow to improve their balance and mobility. In addition, the rehabilitation efforts are facilitated with more effective therapy means made available to specialists, ultimately enhancing their overall quality of life [7, 4].

The device designed in this project is a unilateral active hip orthosis. Orthoses may sometimes be mistaken with prostheses. These two assistive devices do not share the same function since an orthosis refers to a technology enhancing and correcting the use of body parts, whereas a prosthesis is an artificial limb to cope with the loss of a limb [8].

1.2 Description of the previous works

This project began with the master's thesis of Guillaumie and Lejeune [9], who focused on the core specifications and initial design of the orthosis. After considering various design options, they chose to use a dual four-bar mechanism as the basis for their solution. They created a prototype using 3D printing, as shown in Figure 1.1.

The transmission mechanism chosen was a direct-drive transmission with a planetary gearhead, connected to the Maxon motor EC60 flat. They also incorporated the option to attach a parallel spring, which would store energy during hip extension and release it during flexion to reduce the motor torque. The device was controlled using an EPOS2 driver and a myRIO controller, along with a LabVIEW program. The assistive force was measured using a 6-axis force/torque sensor. However, due to delivery delays, they had to use a less efficient motor and planetary gearhead for their tests.

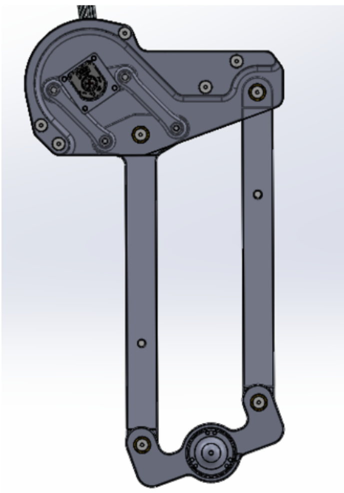

Figure 1.1: Initial orthosis design from Guillaumie and Lejeune [9].

Camille Pestiaux [10] continued the work in her own master's thesis. She integrated the missing components from the original design and developed a wearable prototype by designing a corset. The corset allowed for safe use by a healthy subject while enabling adduction/abduction movements. Figure 1.2 shows the hinge mechanism, the hip interface, the transmission, and the actuation assembly of Pestiaux's prototype.

Pestiaux further improved the original design, including a change in sensor selection. She aimed to achieve a transparent mode where the orthosis would provide zero assistive force but with the future objective of providing a slight impulse during hip flexion. She implemented a feedback loop using a PID controller to adjust the force asked based on the comparison between the measured force from the sensor and the desired force setpoint. Two limit switches were used to control the angular movement permitted, set at the maximum hip extension and flexion allowed by the orthosis. The switch accounting for the extension limit was used for the 0° initialization. Although she successfully created a working wearable device, there was still a high residual force during the transparent mode, and the current reached saturation.

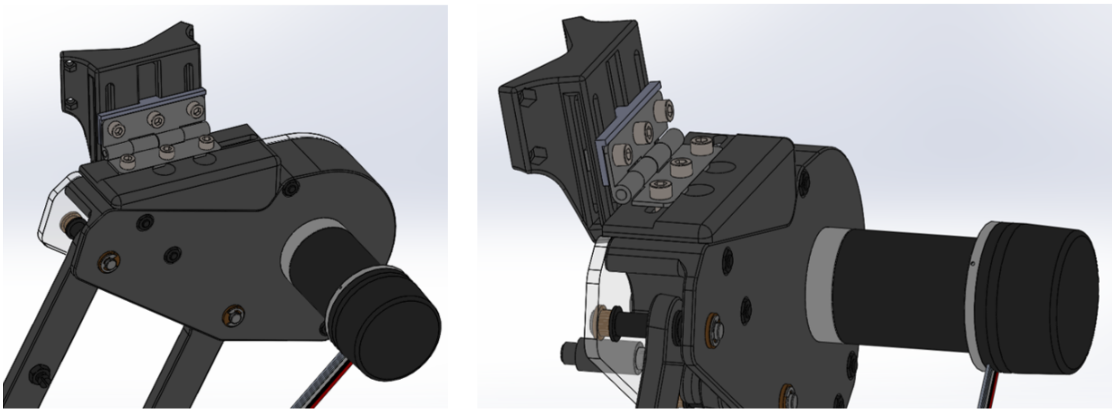

Figure 1.2: Hip level interface of Pestiaux's prototype [10].

In his master's thesis, Julien Desbrosses [11] focused on redesigning the action chain to minimize internal friction losses, which were hindering the motor's ability to accelerate quickly enough and follow the hip movement. Desbrosses aimed to achieve an assistive torque of 40% of the biological torque to avoid destabilizing the wearer.

The new version of the transmission chain used a pulley-belt system with a tensioning roller, as shown in Figure 1.3. Its new solution replaced the secondary four-bar mechanism designed by Guillaumie and Lejeune [9], turning the system into a single four-bar mechanism. The motor was relocated to the rear of the corset to eliminate parasitic torque on the side of the hip. Figure 1.4 illustrates the new orthosis design, which was also 3D printed.

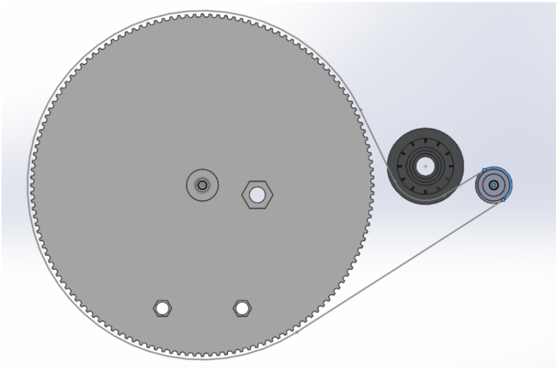

Figure 1.3: Pulley-belt transmission system [11].

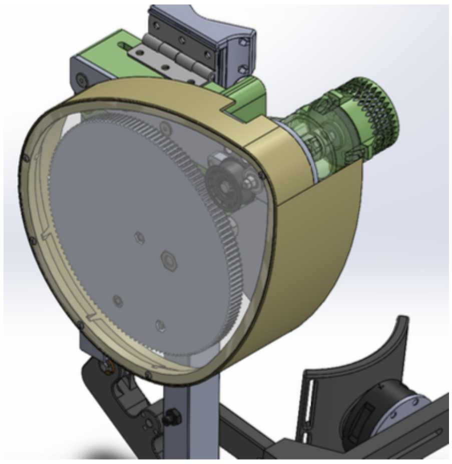

Figure 1.4: New orthosis design from Desbrosses [11].

Following Desbrosses, Nicolas Sturam contributed to the project during his master's thesis [12]. In the first part of his work, Sturam focused on improving the ergonomics of the device. He made changes to the fastening system of the corset and enhanced its comfort, as depicted in Figure 1.5a. Additionally, the electronics were gathered together and fixed on the back of the corset, allowing for shorter cables and minimizing the risk of accidents, as shown in Figure 1.5b.

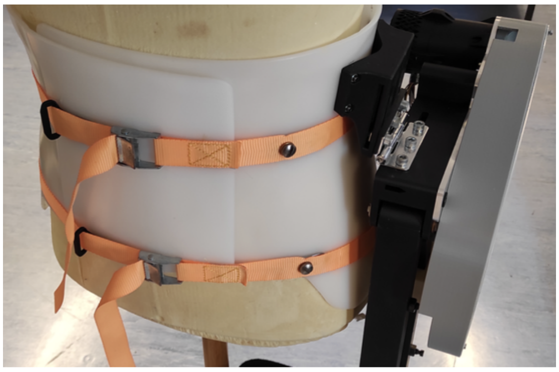

(a) Corset fastening - front view.

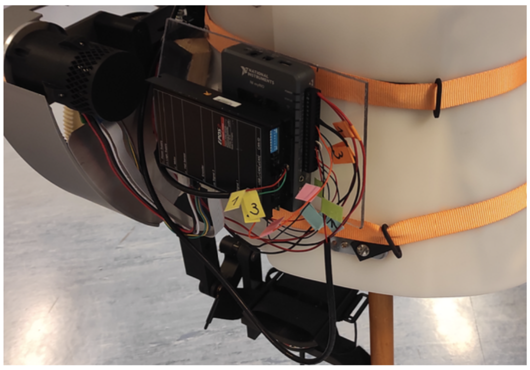

(b) Electronics support - back view.

Figure 1.5: Sturam's design improvements [12].

The second part of Sturam's work involved improving the controller. He addressed remaining bugs in the existing architecture and attempted to implement an adaptive force profile to assist patients. However, this task produced unsatisfactory results, with significant delays when learning the wearer's walking cadence. Sturam also noted current saturation, which prevented the orthosis from reaching the desired assistive torque.

1.3 Goal of this work

During this master's thesis, the main goal was to design a functional control of the assistance delivered by the orthosis. Two main aspects needed to be considered: the ability of the controller to synchronize with the patient's pace and its versatility in the assistive force produced to meet the user's needs. The implementation process was divided into two parts, splitting the two main requirements to be designed independently. The first focus was to detect the cadence with minimum latency and extract gait parameters of interest from the wearer's hip angular displacements. This phase had to be able to dynamically follow changes in walking patterns and continue being in phase with the subject. As for the second focus, it was about designing a periodic force profile to be delivered along the gait cycle. As the assistance level is not constant for every user, nor for every task, the force had to be configurable with respect to certain relevant features.

Several electro-mechanical issues had to be remedied too. Among other topics, the wiring organisation had to be rethought for more robustness and the main current saturation problems needed to be fixed. In addition, the parallel spring integration had to be rendered practical without causing any current overflow for the device, nor hindering the wearer's walk.

Lastly, experimental assessments of the device on a sound subject were carried out. Multiple features were investigated going from the corset comfort and configuration to the optimum assistance settings. The orthosis performances were analysed and compiled as per the goals of this project.

Chapter 2

State of the art

2.1 Gait analysis

Hip degrees of freedom. The hip joint is a ball-and-socket connecting the femur to the pelvis. This gives the joint three degrees of freedom (DOFs) consisting of the rotations in all three anatomical planes [13]. The planes and axes of reference for the human body are shown in Figure 2.1 and the three rotational DOFs of the hip are illustrated in Figure 2.2.

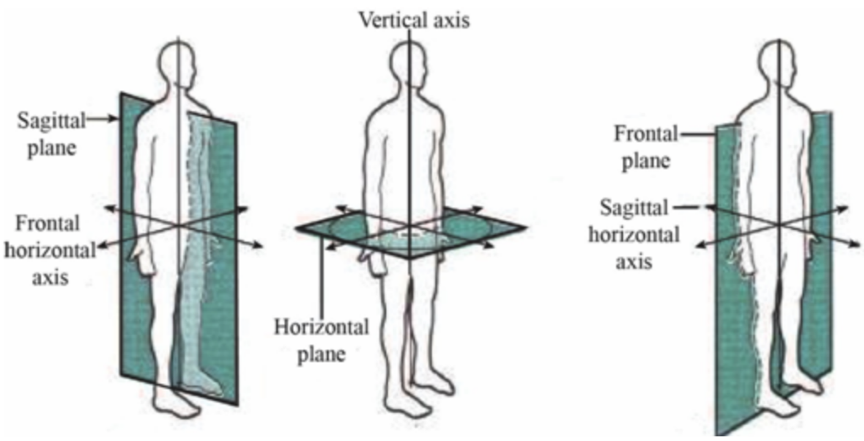

Figure 2.1: Human body anatomical planes and axes [14].

The extension and flexion rotations account for motion in the sagittal plane, the abduction/adduction ones occur in the frontal plane, and the external/internal rotations take place in the horizontal plane. The orthosis focuses on the **flexion/extension** movements to recreate a normal gait but the **abduction/adduction** rotations are also enabled by the device.

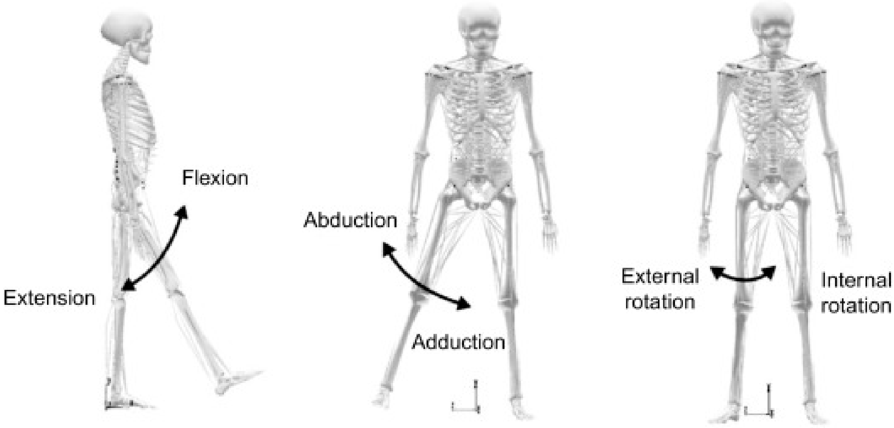

Figure 2.2: Hip joint degrees of freedom [13].

Gait cycle stages. A gait cycle is the timeline between two successive occurrences of the same event of the walk. The initial contact of one foot with the ground usually defines the starting point of a cycle. During a cycle, the leg (that initiated the gait cycle) goes through seven stages, as shown in Figure 2.3. This part is mainly based on the work of Whittle [15].

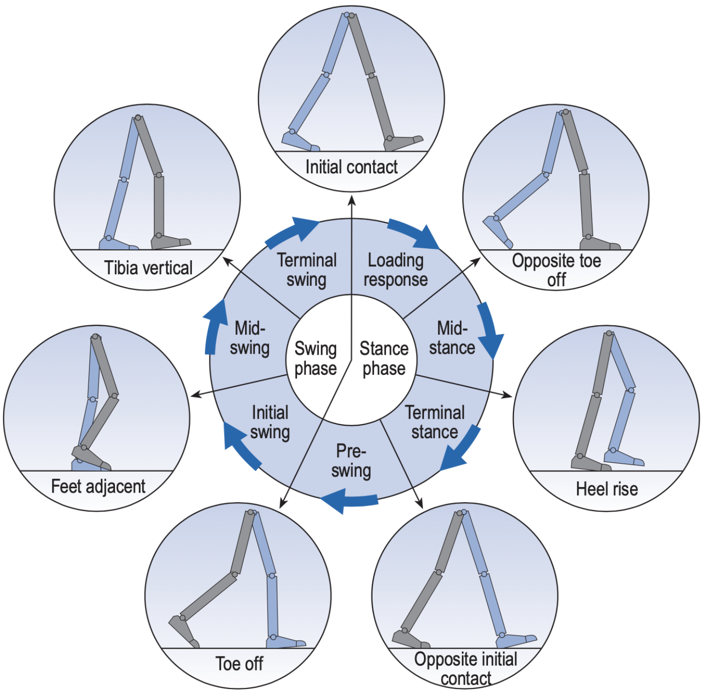

Figure 2.3: Gait cycle timeline for the right leg (gray) from [15].

The other leg goes through the same series of events but offset by half a cycle. The coordination between both legs is illustrated in Figure 2.4. The timeline shown starts with the right foot initial contact.

The seven stages can be divided into two series of events. The first one is called the "stance phase" and includes all the stages where the foot of consideration is in contact with the ground, from the initial heel strike to the toes leaving it. Of the seven total periods, four are covered in this first phase:

- **Loading response:** first stage of the cycle, beginning with the ground contact initiated by a heel strike and ending with the opposite toe off. This transition from one leg off-ground to the other represents the first double support period of the gait cycle.

- **Mid-stance:** this period is characterised by a single support from the leg of consideration with the transition of the hip position from a flexed one to an extended one. It takes place after the opposite toes left ground and before the heel in contact with the ground rises, initiating the foot lift.

- **Terminal stance:** second half of the single support from the leg of consideration. It begins with the heel lifting off and ends with the opposite heel strike, transitioning to another double support period. During this stage, the foot with ground contact continues its rise.

- **Pre-swing:** this stage concludes the stance phase with the end of the ground contact from the considered foot. This is also the second double support period of the gait cycle with the opposite foot initiating its own stance phase. The period ends with the toe off, giving place to the second phase of the gait cycle. During this stage, the hip undertakes the flexion movement which will bring the foot forward during the swing of the leg.

The second series of events of a gait cycle is called the "swing phase". This phase corresponds to the part where the foot moves forward through the air, whereas the stance phase occurred when the foot was on the ground. The last three periods of the seven total ones are included in this second phase:

- **Initial swing:** after the toe off event, the foot initiates its forward displacement thanks to the flexion from the hip. This period ends when the foot catches up with the opposite one, leading to the feet adjacent event and marking the beginning of the next period. At this point, the hip already reached a 20° flexion angle.

- **Mid-swing:** during this period, the hip continues flexing until the tibia reaches a vertical position. The flexion ceases and the swing can enter its last stage before undertaking another cycle. The ankle starts dorsiflexing during this stage, preparing for the heel strike ending this cycle.

- **Terminal swing:** last period of the whole gait cycle, bringing the foot back to the ground with the heel strike initiating the contact. The hip do not rotate anymore, only the knee and ankle do. The knee starts to extend, moving from a flexed position to an extended one, while the ankle, on the other hand, continues its dorsiflexion which brings the foot closer to the ground.

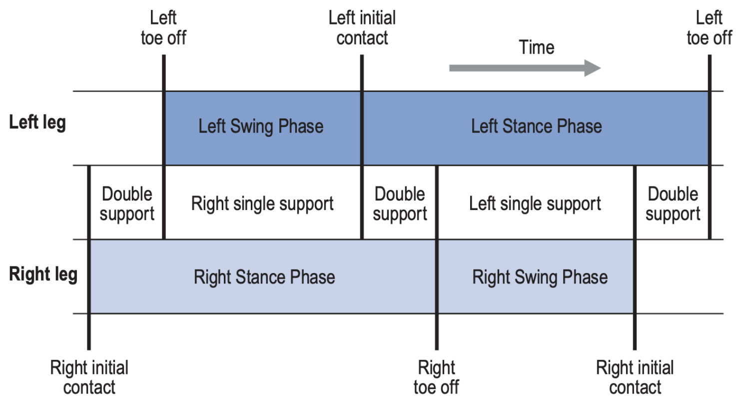

Figure 2.4: Gait cycle timing for both legs from [15].

The hip joint angle is shown in Figure 2.5a, while the moment of the joint is plotted in Figure 2.5b. The torque data come from Winter's work [16] which had been used to set the goals of the orthosis.

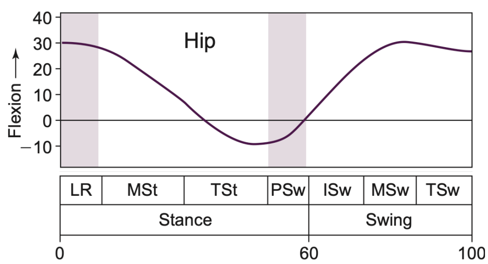

(a) Hip joint angle from [7].

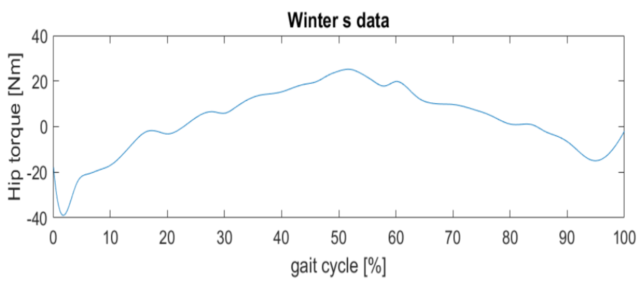

(b) Hip joint moment from [11, 16].

Figure 2.5: Biomechanical data for the hip joint during a gait cycle. LR, loading response; MSt, mid-stance; TSt, terminal; PSw, pre-swing; ISw, initial swing; MSw, mid-swing; TSw, terminal swing.

Hemiparetic gait. Hemiparesis can occur after a lesion of the central nervous system (CNS), either at the brain level or at the spinal cord and nerves level [17]. The most common cause is a stroke. It generates a weakness in all or most of the anatomical segments of one side of the body. It has consequences on both the affected and sound sides with a decreased stance time for the affected leg and a shortened step length for the healthy one. A stiffness can also be observed in the affected limb [7].

The pathological gait differs from the normal one mainly by the weakness in dorsiflexion and the excessive plantarflexion of the ankle which can lead to instability. A second abnormality comes from the reduced hip and knee flexion [7, 18]. The hip joint moment of an hemiparetic gait compared to a normal gait is shown in Figure 2.6.

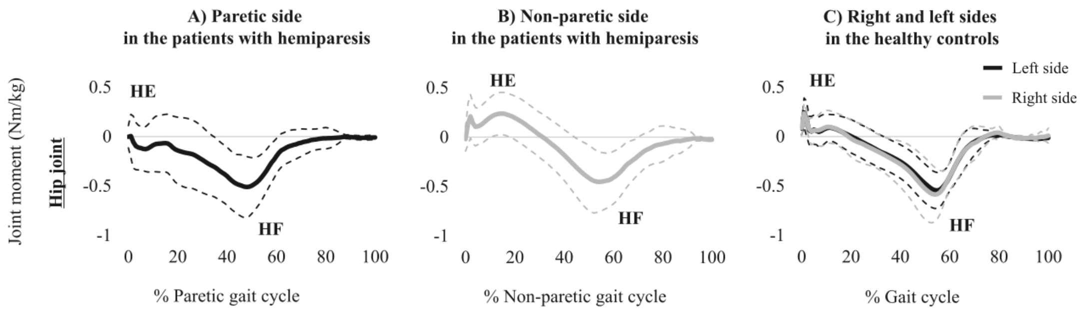

Figure 2.6: Hip joint moment in the sagittal plane with hemiparetic subjects compared to control ones, from [18]. Average (solid line) and ±1SD (dashed lines) moments. HE, hip extension; HF, hip flexion.

2.2 Control strategies for assistive devices

2.2.1 Biological gait controller

Before designing a controller for an active hip orthosis, it might be important to first study the biological gait controller of the human body. Indeed, understanding the foundations underlying the human controller allows to design controllers working with the user in a synergistic way, leading to assistive devices that are more intuitive and comfortable for the users. This section gives a quick overview of the biological gait controller working principles based on the works of Tucker et al. [19] and Prochazka and Geyer [20].

The human locomotion is controlled by nature's most optimized controller, the central nervous system (CNS). The CNS is responsible for processing sensory information and orchestrating motor functions. It encompasses the brain and the spinal cord, as well as the nerves. A diagram of the control system is shown in Figure 2.7; the system can be analysed in parallel with the hierarchy proposed by Tucker et al. [19] for a biorobotic controller, as shown in Figure 2.8 from Section 2.2.2. The three theoretical layers of the controller as described in their work are highlighted in the diagram. They can also be referred to as the supraspinal level (or cortical level), the central pattern generator (CPG) from the spine and the musculoskeletal system.

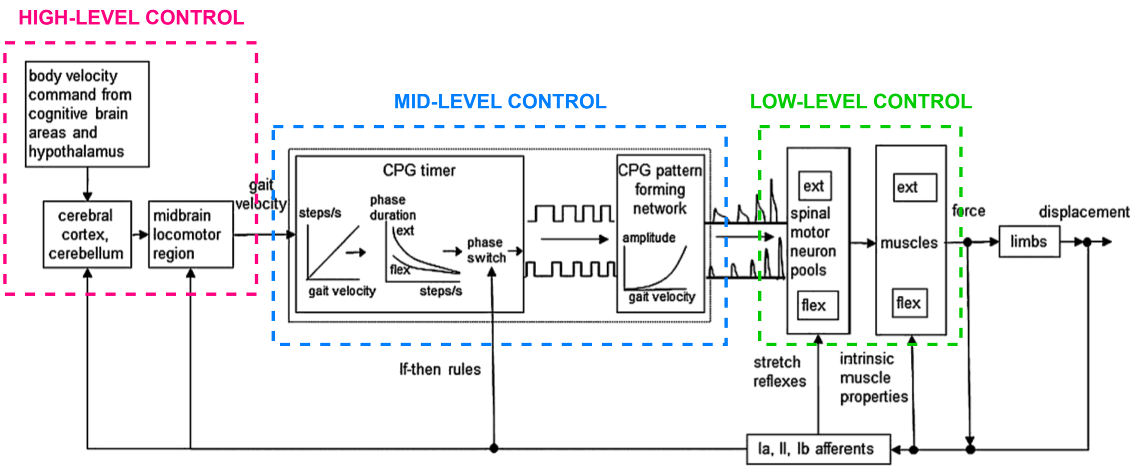

Figure 2.7: Biological locomotion control system synthesised with comparison to the three controller layers, adapted from [20].

Supraspinal level. The supraspinal areas govern the locomotion intents by adjusting the gait velocity of the body. The velocity is estimated regarding the goals set cognitively, exteroceptive inputs (vision and other senses), and proprioceptive inputs from bodily mechanoreceptors.

Central pattern generator. The CPG is a network of interneurons who are thought to generate basic rhythmic motor patterns. Its action is regulated by the supraspinal level which modulates the body velocity. The first component of the CPG manages the phase duration, while the second one computes the activity levels of flexor and extensor muscles.

Musculoskeletal system. Given the activity levels generated by the CPG, the α-motoneuronal pools activate the flexor and extensor muscles adequately. As for a assistive device low-level controller, the activation is regulated by a feedback loop (afferent feedback from muscle spindles, Golgi tendon organs, mechanoreceptors and nerves).

Feedback loops. Every layer of the biological controller are regulated by feedback loops from multiple means. The intrinsic stiffness of the muscles provides immediate feedback at the end-effector level. The motoneurons take feedback from the muscle spindles which alert when a muscle is stretched due to a change in the joint position; the action can be adapted to prevent from overstretching and help maintain a stability. The phase switches (between stance and swing phases) in the CPG are controlled by rules that use sensory feedback to estimate the gait cycle state. The supraspinal level also receives feedback from sensory input to adapt the overall commands.

2.2.2 Overview of biorobotic controllers

The controller of an active orthosis can be seen as the brain behind the operations. It controls the whole device and governs its behavior. Given inputs from various sources, it will map the device state with the user's intentions and generate an adequate output. In other words, it serves as a link between the human and the mechanical action, while taking into consideration the external conditions.

Tucker et al. [19] proposed a general framework for the control of active lower-limb prostheses and orthoses, as shown in Figure 2.8. It highlights the physical interactions between the device, the user and the environment, as well as the signals exchanges between the different entities. The diagram also structures the controller into three layers:

- **High-level:** also called the "perception layer", this level aims at perceiving the user's intentions and recognising the locomotion task, such as standing, walking, climbing stairs, and more. It is also possible to allow the user to voluntarily control the device's state with the direct volitional control. After having estimated the wearer's desired action, the goal is transmitted to the mid-level layer through means such as a trajectory, velocity, and other relevant parameters.
- **Mid-level:** also known as the "translation layer", the goal here is to apply a control law on the user's stare within the gait cycle to compute the desired device states to be tracked by the low-level layer. The new device states are determined based on the intentions previously estimated by the high-level controller, they may take the form of a position, torque, impedance setpoints and more.

- **Low-level:** also referred to as the "execution layer", it computes the error between the desired device states and the current ones, thanks to feedforward or feedback control loops. It then adjusts the command delivered to the actuators in order to achieve the action aimed.

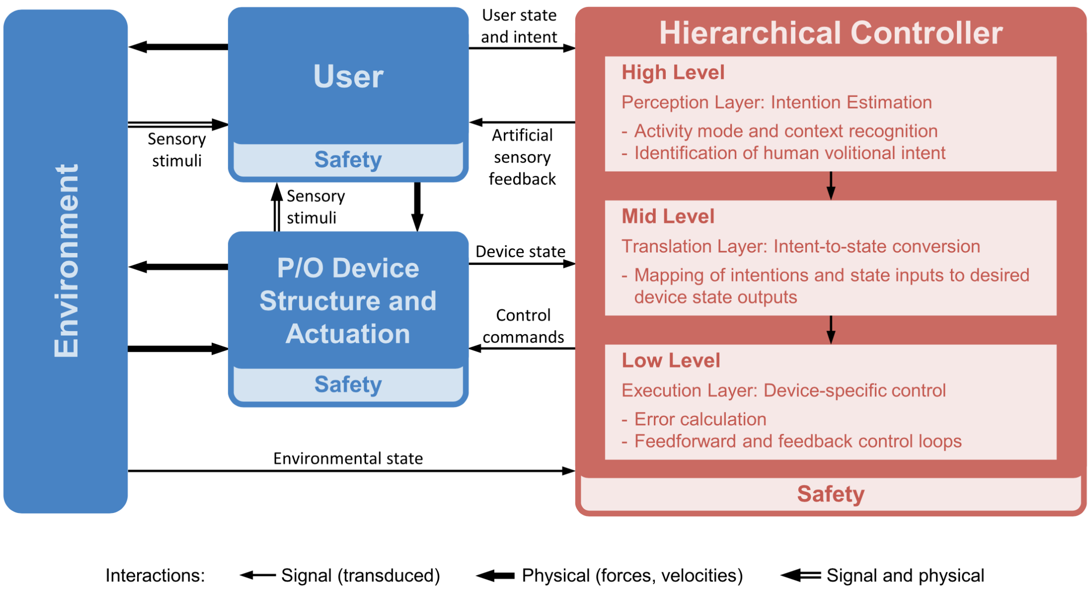

Figure 2.8: Controller hierarchy and interactions for active prostheses and orthoses designed for lower limb impairments, from [19].

2.2.3 High-level controller and intention estimation

The goal of the high-level controller is to estimate the user's intentions. Tucker et al. [19] described it as the combination of an activity mode detection and direct volitional control from the user. In their work, they gathered the main methods used in the literature. This section is mainly based on their work as well as the work of González-Vargas et al. [21] who relate the latest advances in the field of wearable robotics.

Activity mode recognition

This feature of the high-level controller refers to its ability to identify and classify the current task of the user in order to adapt the commands delivered to the mid-level controller. When designing a gait assistive device, it is important to adequately support different tasks. Indeed, the assistance delivered to climb stairs should not be the same as the one used when walking forward. The high-level controller therefore has to detect changes in activity modes so the mid-level controller can select the right control law for the situation.

Task classification. Two methods are frequently used to design a classification model for the controller:

- **Heuristic rule-based classifiers:** this first method makes decisions based on a set of predefined rules to classify the current activity given data from sensors. Typical algorithms are finite state machines and decision trees. However, as the classifier needs to make a decision within a certain set of different activity modes, they are limited by the few activities implemented and do not have the ability to adapt to other situations. In other words, heuristic rule-based classifiers requires to manually define rules based on previous knowledge to categorise sensor data into activity modes. Each activity has specific control laws in the mid-level controller.

- **Automated pattern recognition:** whereas the first method used a set of rules determined manually and lack the ability to dynamically enlarge its range of activity modes, this second method uses machine learning and statistic fields to automatically create a larger range of activities. The relationships and rules between the different modes are learned by the system during supervised training. The patterns can therefore be more complex than previously and the system can take into account more relevant features from the sensors. While it takes time to train such an algorithm, the decisions should ultimately be more accurate than for the heuristic rule-based approach. Frequent techniques used to build the model are neural networks, support vector machines and random forests.

  Example: Accogli et al. developed a machine learning algorithm to detect the user's intentions with the assistive upper-limb exoskeleton NESM [22]. This exoskeleton provides four active degrees of freedom, and a wide range of actions that could not be easily manually classified into fixed activity modes. Their controller learned the different patterns based on electromyography signals. They combined a Gaussian Mixture Model and Support Vector Machines to estimate the motion intentions and directions.

Input means. The data used in these different classifiers can come from many sources. Of course, the device can use more than one source. Here are means commonly used in the active orthoses field:

1. **Embedded mechanical sensing:** they provide information about mechanical parameters like joint positions, torques and velocities to estimate the device's state.

Example: Robo-ankle exoskeleton by Carnegie Mellon University [23]. This device mimics the muscles, tendons and ligaments of the ankle to assist patients with ankle-foot impairments. The controller uses data from a strain sensor placed on the top of the foot to detect the extension or flexion of the ankle. This strain sensor reminds the stretch reflexes from the biological gait controller.

2. **Body-Worn force and position sensors:** allow to estimate the user's state and joint positions. The initiation and termination of movements can be detected by changes in the force interactions with a force sensor or joint positions.

   Example: Lokomat orthosis by Hocoma. It is a robotic device designed to assist the gait of impaired patient in rehabilitation. Force sensors are placed between the actuators and the user on strategic locations to measure the hip and knee joint torques [24].

3. **Sensing of cortical activity:** by capturing brain signals, patterns can be found to detect the intentions as they are initiated by the brain.

   Example: Lee et al. [25] developed a classification model able to discern intentions from electroencephalogram (EEG) recordings. By placing an active electrode system on the scalp of the subject, they achieved to control the Rex lower-limb exoskeleton from Rex Bionics [26]. They chose to experiment of this exoskeleton for its ability to move independently without the support of the user.

4. **Surface electromyography (EMG):** the muscle activity is used to detect motion intentions even before any movement can be observed.

   Example: HAL (Hybrid Assistive Limb) by Cyberdyne. This assistive lower-limb exoskeleton uses EMG signals to modulate its assistance. This technology allows better interactions between the user and the device. This device is also a great example of the combined use of different input means for control as it also records neural signals [27].

Other input means used in the field of active lower-limb orthoses include environmental sensing (gyroscopes, infrared sensors and sonar sensors, among other technologies), movement of the center of pressure/gravity monitoring, neuromuscular-mechanical fusion and manual mode switching.

Direct volitional control

When designing the controller of an active orthosis, it can be useful to implement a control strategy that allows the user to directly command the device. Along with an activity mode recognition classifier for autonomous assistance during cyclic and locomotive activities, this second control strategy handles the irregular activities.

2.2.4 Mid-level controller and intention translation

As a reminder, the mid-level controller receives its instructions from the high-level controller after having determined the activity to enhance. Its purpose is to translate the locomotive intent (estimated in the form of motion features like a trajectory or a velocity) into a desired device's state. In other words, it takes displacement parameters and turns them into corresponding device-specific setpoints. To adequately deliver gait assistance, the mid-level needs to compute the device current state and take it into account. Controllers can also have multiple mid-levels, one for each activity mode to design specific control laws, for example. The output of the mid-level is used by the low-level controller to operate the actuators.

Once again, this section follows the work of Tucker et al. on active lower-limb robotics [19]. In their work, they sorted the mid-level controllers in two classes: phase-based and non-phase-based.

Dynamic phase estimation

- **Adaptive Frequency Oscillator (AFO):** the frequency component of the input signal is learned by using in parallel some oscillators. It can be seen as a kind Fourier decomposition in real-time. A feedback structure is used to update the result at each time step, making each oscillator converge to the frequency components of the signal. Each variable (frequency, amplitude and phase) of each oscillator needs to be set beforehand. They have a significant impact on the convergence of the system, an improper initial setting may lead to bad performances [28]. They were invented by Righetti et al. [29].
- **Adaptive Oscillator (AO):** the convergence of AFO is improved based on the assumption that the input signal is periodic (as is the gait). The fundamental frequency of the signal is shared by the oscillators, reducing the number of variables requiring to be set at the beginning. The performances are therefore enhanced [28]. This improvement of the AFO was proposed by Ronsse et al. [30].

Phase-based control

- **Trajectory control:** the trajectory of the actuated joints is predetermined based on patterns defined for each activity modes considered by the device.

The trajectory can sometimes be modulated by the gait velocity and physical characteristics of the user.

Example: Kapti et al. developed a trajectory-based controller for a knee prosthesis by predefining basic life patterns. However, the patient's freedom was limited by the number of patterns used [31].

- **Echo control:** the other limb kinematics are recorded and repeated on the affected limb with a certain time delay. The goal is to symmetrize the gait. This method allows for a more intuitive control of the device by the user.

  Example: the Power Knee prosthesis from Össur which uses the sound limb posture and the gait cycle phase to determine the required position of the replaced knee and sends this information to the actuators [31].

- **Finite-state controllers:** they consider the gait cycle as a series of consecutive phases with a different assistance profile for each one of them. The transitions are event-triggered. Each activity mode from the high-level classifier has its own state machine which increases the complexity of the controller, especially when the number of activities or gait phases considered is high. This represents one of the main drawbacks of this approach.

  Example: the BioMot ankle exoskeleton [32] uses a state machine to determine the lower levels control laws. The state switches are triggered by changes in the joint torque and angle. Three states govern the action of the device, as shown in Figure 2.9. This allows to use three different control strategies, one for each state, and exploit a system to store the energy during a certain state in order to later release it for the push-off phase of the gait.

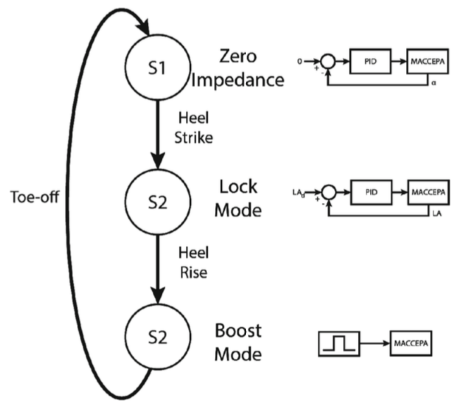

Figure 2.9: BioMot control strategies [32].

Non-phase-based control

- **Complementary limb motion estimation (CLME):** method very similar to the echo control one by the fact that they both record data from the sound limb. The difference comes from the phase importance. Indeed, the echo control uses the gait phase detection from the sound leg to synchronise the affected one (with a time delay), whereas CLME continuously estimates the desired action from real-time data from the sound limb.

- **Force-feedback control:** particularly useful for transparency control, this method consists in reducing the interaction force measured by a sensor placed between the user and the orthosis.

2.2.5 Low-level controller and intention execution

The last layer of the controller's structure as proposed by Tucker et al. [19] is the low-level. This is were the actuators' commands are computed to carry out the action determined by the higher levels. The low-level tracks the device's state by feedback and feedforward loops to drive the actuators in order to reach the desired state, reducing the error between the required and actual actions. As the orthosis being designed in this work has a functional low-level controller already implemented, this section only consists of a quick review of the state of the art drawn by Tucker et al. in their work [19].

- **Feedforward control loops:** it consists in the anticipation of the system's future state. By providing the controller with information about expected inputs, it can adjust the command sent to the actuators in prediction of the foreseen events. This approach allows to minimize the impact of disturbances without relying solely on the feedback control loops to react when they occur. However, this method may be difficult to implement given that it requires a model of the system's interactions.

- **Feedback control loops:** by taking as inputs the system's performance data in real-time, the controller compares the actual outputs to the desired setpoints and adjusts the commands adequately to reduce the differences. This approach provides the controller with the ability to quickly react to unforeseen events and handles unpredictable disturbances to maintain stability. The mechanisms frequently used are P, PI, PD or PID controllers (P stands for proportional, I for integral, D for derivative, and they account for the different control actions implemented).

Chapter 3

System description - orthosis presentation

3.1 Overview of the current solution

Figure 3.1 gives an overview of the orthosis architecture. To provide an assisting torque to the wearer's leg, a four-bar mechanism is actuated by a motor and controlled by a driver. This section summarizes the current solution and its working principles. As stated before, this project is the result of multiple thesis works [9, 10, 11, 12]. The main contributions made during this work are progress on the controller and ergonomics improvements.

The orthosis having never been named in the past, it was time to finally find one. Among different names suggested and submitted to a vote, one of them unanimously stood out from the list. Meet H.E.R.O., the Hip Empowering Robotic Orthosis.

As stated in Section 1.2, Desbrosses quantified the required assisting torque delivered by the orthosis to 40% of the biological torque [11], which corresponds to $10.2[Nm]$ according to Winter's data [16]. This data has been collected on healthy subjects at a gait velocity of $0.8[\frac{m}{s}]$, which is in between the characteristics for a healthy elderly and an elderly having suffered a stroke. A lower bound for the aimed torque has been arbitrarily set to 20% of the biological torque, corresponding to about $5[Nm]$.

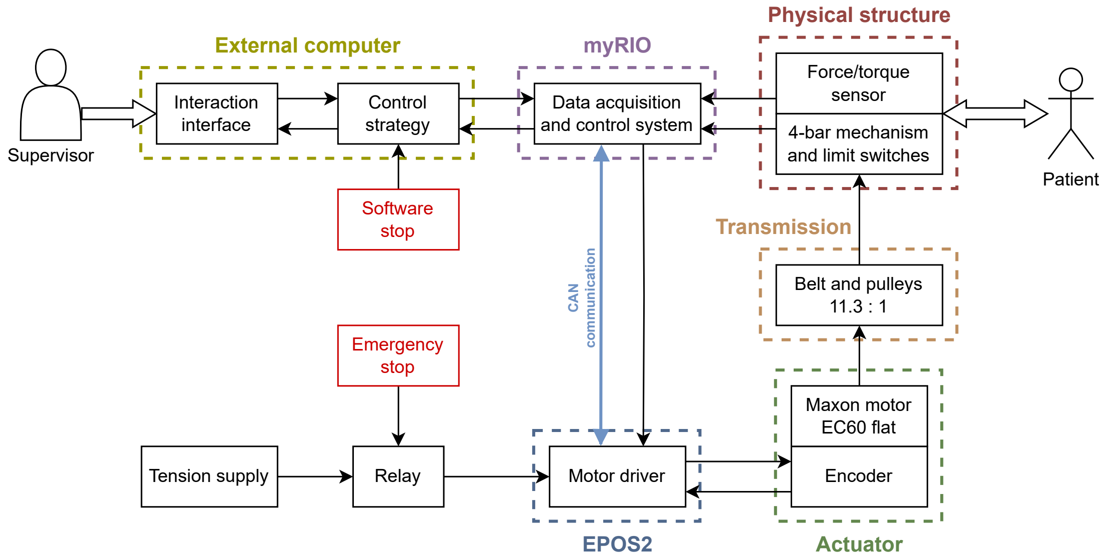

Figure 3.1: Orthosis general architecture and interactions between the different components.

The orthosis can be split into two parts: the mechanical part and the electro-mechanical one. The first part is composed of the orthosis structure and transmission means, while the second part is divided into the actuator, the driver EPOS2, the controller myRIO and the computer blocks. The interactions between the different blocks are represented in Figure 3.1.

3.1.1 Mechanical transmission

Four-bar mechanism. The H.E.R.O. orthosis is designed to enable two degrees of freedom to the hip: adduction/abduction and flexion/extension. A schematic representation of the main mechanism is shown in Figure 3.2. It is composed of a four-bar system linked to the hip of the wearer on one end, and to the back of his thigh on the other end (via the green revolute joint). The top bar (i.e., the fixed frame bar) is connected to a hinge fixed on the corset, accounting for the adduction/abduction movements in the frontal plane. Of the four revolute joints forming the four-bar structure, the actuated one is located at the rear of the hip (joint between the fixed frame bar and mobile crank bar). The flexion/extension movements in the sagittal plane are driven by the crank rod [33] and the prototype is designed to achieve a range of motion of 110°, delimited by two limit switches (integrated to the frame).

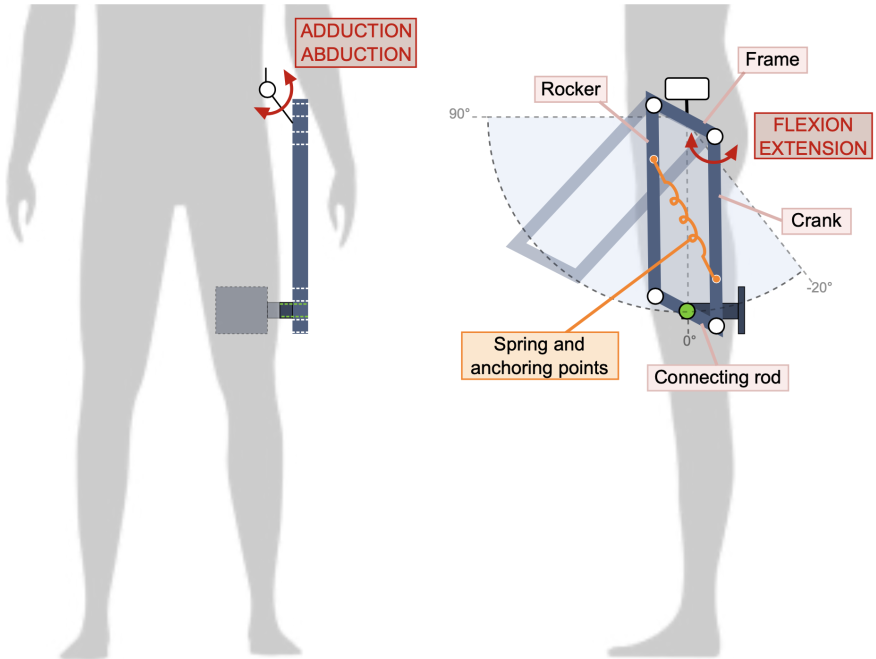

Figure 3.2: Schematic representation of the four-bar system with the addition of the parallel spring.

The distance between the point of torque production and the point of application of the generated force is $0.28[cm]$. The torque produced τ_m according to the force applied F is then:

$$\tau_m = F \cdot 0.28 \tag{3.1}$$

Pulley-belt system. The next element on the transmission chain is the pulley-belt system, preceding the motor shaft. In his work, Desbrosses designed a system composed of two pulleys, a large one and a smaller one (i.e., the actuated one), and a timing belt tensionned by a tensioning roller [11]. Their configuration is shown in Figures 3.3 and 3.4. The reduction ratio achieved by the pulleys of the belting system is 11.3:1.

Parallel spring. Lastly, a parallel spring can be added to provide more assisting force. The two anchoring points and the spring are represented in orange in Figure 3.2. With this configuration, the torque curve can be offset, resulting in less power need to achieve the required torque and, therefore, a cheaper and smaller motor. The spring has a neutral length $l_0 = 0.15[m]$ and a rigidity constant $k_p = 1400[\frac{N}{m}]$, its specifications can be found in Appendix B. The impacts of the spring are studied

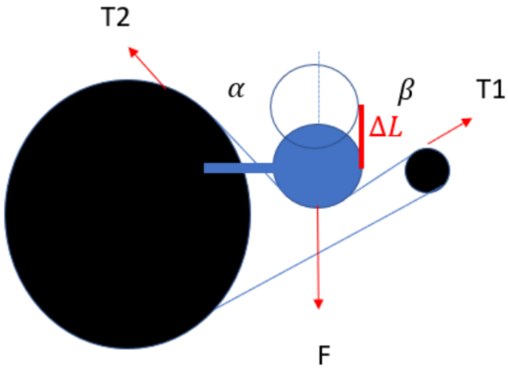

Figure 3.3: Belting trigonometry. Pulleys are in black; the tensioning roller is in blue: initial position when not filled, filled circle is after applying the initial tension [11].

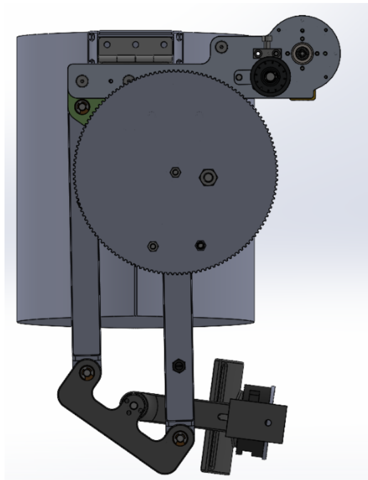

Figure 3.4: Assembly of the transmission system elements, without the spring [11].

in Section 5.2.3. However, this configuration restrains the wearer's mobility as the spring is extended in the upright position but reaches its initial length during the hip flexion, blocking the movement. It is therefore not possible to sit or climb stairs when it is mounted.

3.1.2 Electro-mechanical design

Motor shaft. The transmission chain ends with the motor shaft being connected to the small pulley of the belting system. Its block diagram is shown in Figure 3.5. The motor chosen for H.E.R.O. is the EC60 flat from Maxon Motor [34], with an integrated encoder. Since it has an open outer rotor, a cover has been designed for safety measures. Although this cover is screened to allow air to pass through, the assembly still overheats after long uses.

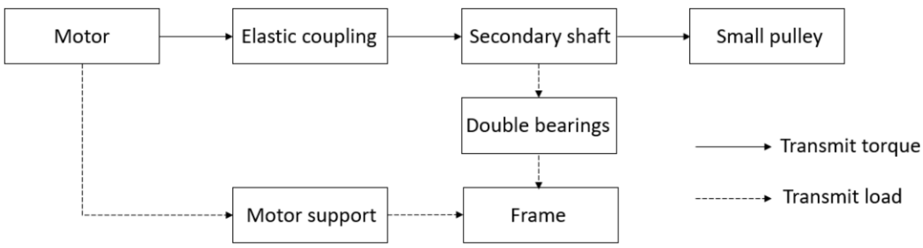

Figure 3.5: Motor shaft [11].

Controller overview. The motor input is given by the driver, taking place in the controller structure shown in Figure 3.6. The controller governs the operation of the device. The ultimate goal is for it to be autonomous, not reliant on any external instructions from the supervisor (see Figure 3.1). The orthosis controller requires the use of two additional devices: a driver (EPOS2 from Maxon Motor) and the control system myRIO from National Instrument. The driver's role is to regulate the motor action based on the required voltage for the aimed movement. It takes place in a feedback loop using a proportional-integral (PI) current controller to compare the actual motor action based on its current. The action aimed, and therefore the corresponding voltage asked, are determined by the myRIO device.

The myRIO is a reconfigurable input/output device, meaning it can be configured for any intended application and then dictate an output instruction given certain input data. The myRIO allows to implement the orthosis behavior according to mathematical developments and communicates them to the motor through the driver EPOS2. The language used to code the force controller into the myRIO is LabVIEW via an external computer, to be disconnected at the end of the H.E.R.O. orthosis development.

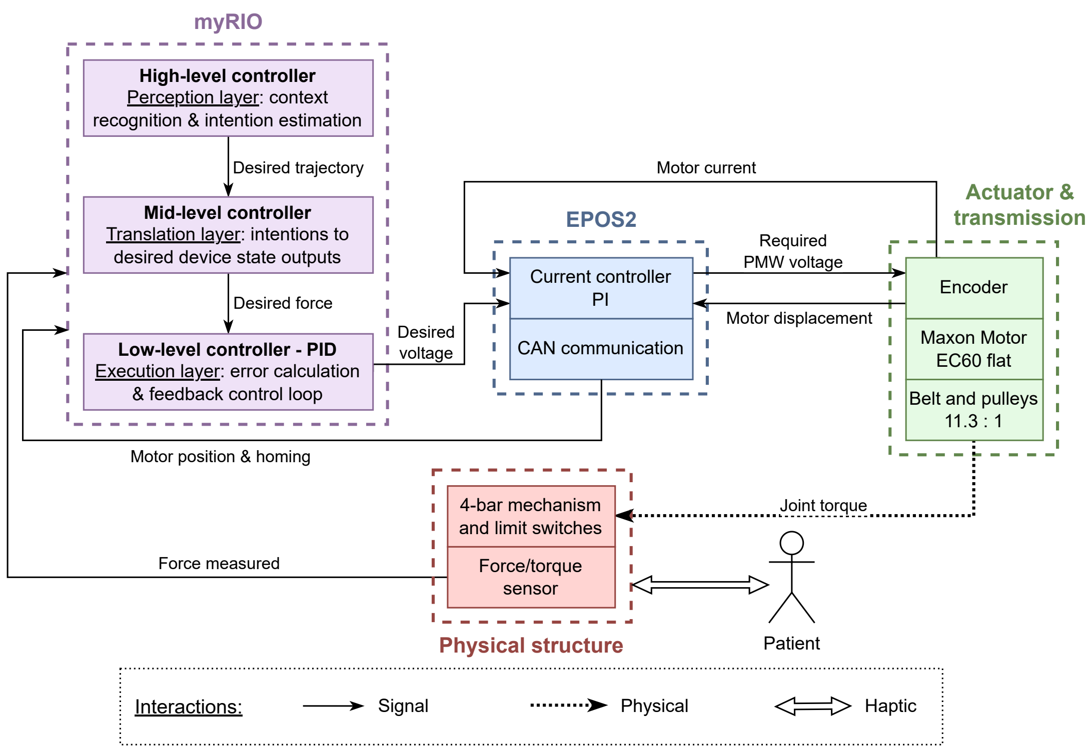

Figure 3.6: Controller block diagram.

Feedback loops and sensor. The information given as an input to the myRIO comes from two sources: the EPOS2 and a force/torque sensor located at the force application point, at the back of the wearer's thigh. The EPOS2 communicates information about the motor variables (via the CAN communication system), while the sensor operates in another feedback loop. Indeed, the force controller from the myRIO adjusts its instructions by taking into account the actual force delivered to the leg in the sagittal plane (the z-direction of the sensor). This second feedback loop is governed by a proportional-integral-derivative (PID) force control.

The sensor chosen is positioned with its x-axis along the vertical axis, its y-axis along the frontal one and the z-axis along the sagittal one, see Figure 2.1 from Section 2.1. It has 6 DOFs, even tough only one is required by the algorithm (the z-direction force). Its x and y directions are used to analyse the parasitic forces on the wearer in order to optimise the orthosis position. Nevertheless, the final version of H.E.R.O. will need to change the sensor by a far more compact one, providing only the required information. Indeed, the current one is quite invasive and adds too much weight on the prototype. Three equations account for the analog calibration of the three forces [10]:

$$F_x = 11.3718 \cdot m - 3.7240 \tag{3.2}$$

$$F_y = 11.3718 \cdot m + 6.4839 \tag{3.3}$$

$$F_z = 11.0698 \cdot m + 9.2952 \tag{3.4}$$

Three layers of control and LabVIEW. As explained in Section 2.2.2, the controller implementation can be divided into three levels:

- High-level controller: task identification by perception of the user's intentions;
- Middle-level controller: given the device's state, applies a control law to effect the intended action;
- Low-level controller: adapt the actuator action based on the desired output and its actual state (feedback loop).

Figure 3.7 shows an overview of the LabVIEW program structure. Detailed diagrams of the main blocks can be found in Appendix A. The low-level controller (summarized in this section) is the result of previous works on the project, while the middle-level controller implementation is this one's goal (detailed in Section 4.1). The high-level controller of the orthosis has yet to be designed.

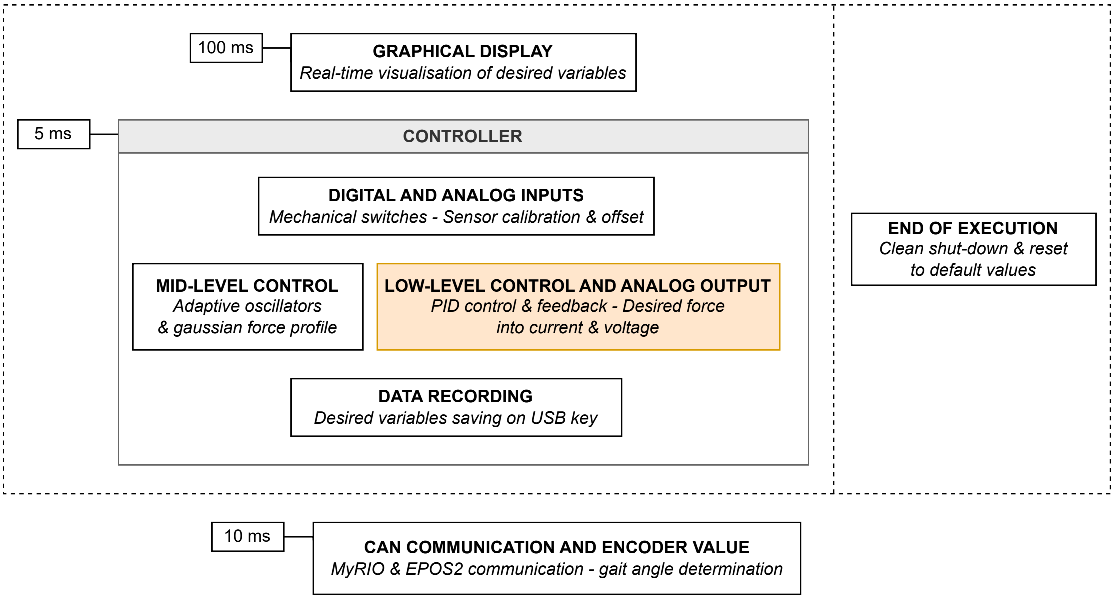

Figure 3.7: Overview of the LabVIEW implementation, highlight of the low-level controller block.

Low-level controller. A schematic representation of the low-level controller implementation is shown in Figure 3.8. The force setpoint is determined by the mid-level controller, while the force feedback comes from the sensor.

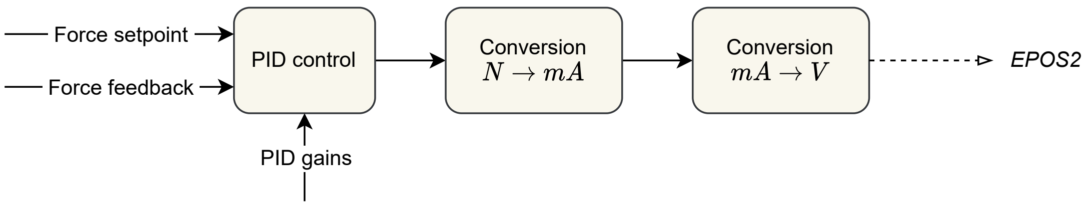

Figure 3.8: Low-level controller implementation in LabVIEW, simplified structure.

The required action from the motor is determined by a PID control law. Currently, only the proportional and integral terms are used, the derivative gain T_D is therefore set to zero. Results from Sturam's work [12] showed that the proportional and integral gains (K_p and T_I, respectively) needed to be tuned. However, as explained in his report, the tuning has to be done manually; traditional methods like the one developed by Ziegler and Nichols do not apply. The manual tuning of the gains was first carried out on a dummy, with the orthosis fixed to its body in order to constrain its movements and have an impedance tending to infinity. This setup allowed to simulate a situation similar as when the device is attached to a human leg but without risking injuring someone. The gains were determined per trial until a stable behavior and a quick response of the prototype was observed. The gains obtained were then refined on a subject. The final values used are: $K_p = 1.2$, $T_i = 0.0005$ and $T_d = 0$.

The force required determined by the PID control is then translated into a current value, before being converted as a tension setpoint sent to the EPOS2. The current needed (in mA) is computed using Equation 3.5, τ_m being the torque to provide ($\tau_m = F \cdot 0.28$, with F the force asked).

$$I = \frac{-\tau_m}{\text{torque constant} \cdot \text{reduction ratio} \cdot \text{efficiency}} \cdot 1000 \tag{3.5}$$

The torque constant is specific to the motor: for the EC60 flat, this constant is $0.0525[\frac{Nm}{A}]$ [34]. As stated before, the reduction ratio of the transmission chain is 11.3, and the efficiency constant has been determined to be around 1 [11]. Finally, the multiplication by 1000 is for the conversion $A \rightarrow mA$, while the -1 factor is for the motor to react in the good direction. The obtained value for the current is then conversed into a tension, after verification that the computed value does not exceed the current limitations (the saturation parameters are set to $\pm 20000[mA]$).

Power supply and hardware specifications. The electronics are alimented by a 35V-20A power supply. Two external stop buttons have been added, one for the wearer and one for the supervisor, in case of an emergency. Another emergency stop has been implemented in the LabVIEW program.

The main characteristics of the motor and driver used for the prototype are gathered in Table 3.1. More detailed hardware specifications can be found in Appendix B.

EC60 flat	
Nominal voltage	24 V
Nominal speed	3480 rpm
Nominal current	7.25 A
Torque constant	52.5 mNm/A
EPOS2 70/10	
Nominal power supply voltage	11 - 70 VDC
Output current, max.	25 A (<1 s)
Output current, cont.	10 A

Table 3.1: Hardware main specifications.

3.1.3 Support and ergonomics

Electronics support. The main ergonomics improvement done during this work concerns the electronics fixation on the corset. In a previous work, Sturam already took upon the task to gather them on a support plate attached to the orthosis [12]. However, the solution designed then appeared to be unsteady, too heavy and needed to be moved to the right (displacement of the center of gravity).

A new support has been created and 3D printed. It has been conceived to be as compact as possible and the 3D printing technique allowed to use a lighter material, the PLA, ending with a final piece weighting 63.6 g. Moreover, the assembly was moved as far to the right as possible (limited by the cable length), with a better distribution of the weight of the whole system. The CAD model is displayed in Figure 3.9 and the final assembly is shown in Figure 3.10b. Other views from the CAD model can be found in Appendix C.

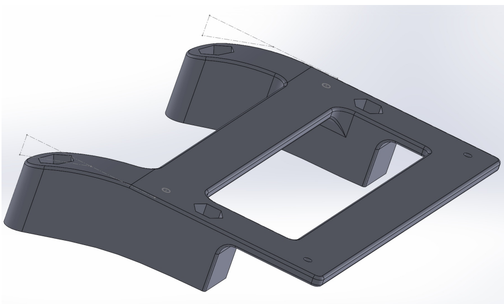

(a) Plain view.

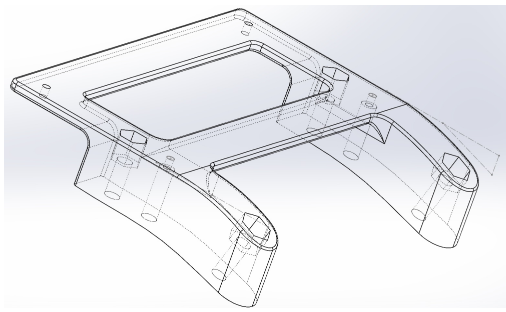

(b) Transparent view.

Figure 3.9: New electronics support, CAD model.

Wiring organisation. A second task was to clean-up and reorganise the cables from the electronics. Some of them needed to be changed, reattached or shortened. In addition, no record of the connections had been drawn up, making it difficult to identify the cables and put them back in place in case they detached. Figure 3.10 shows the evolution of the electronics organisation.

Every cable has been labeled and an Excel file gathering all the required information about the wiring has been created and placed in the external computer of the orthosis. A sheath has also been fitted over some cables to protect and group them. Lastly, a switch has been build for the sensor signals since three of them are retrieved but the myRIO only allowed for two entries.

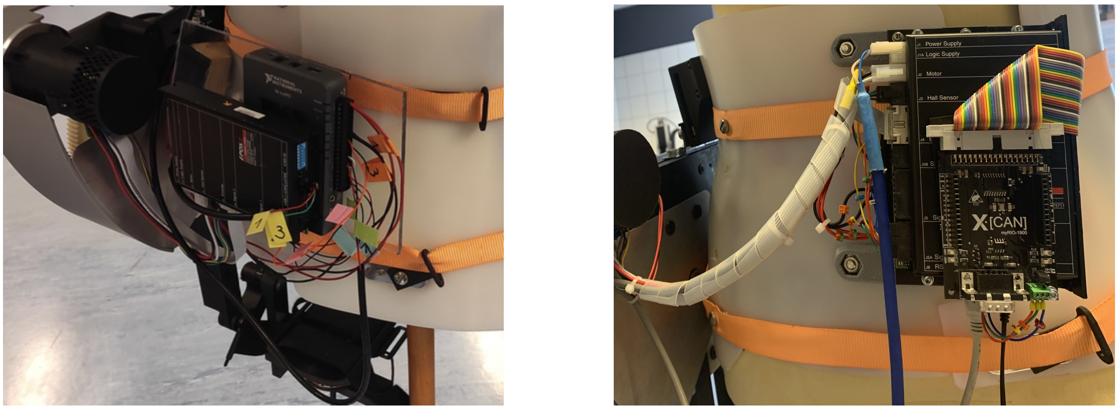

(a) Before changes [12]. (b) Current solution.

Figure 3.10: Electronics management: improvement of the support and wiring.

Corset enhancement. The orthosis is placed on the wearer thanks to a corset manufactured by Pestiaux [10]. It stayed unchanged ever since, except for the fixation system which has been improved by Sturam [12]. The corset is lined with foam for the subject comfort. No major changes have been made in this work, only some shape refining. Indeed, it has been cut up at certain places to improve the mobility of the user and be adjusted to the new electronics support piece. The alterations also aimed at removing as much weight as possible without weakening the structure. The final prototype worn is shown in Figure 3.11.

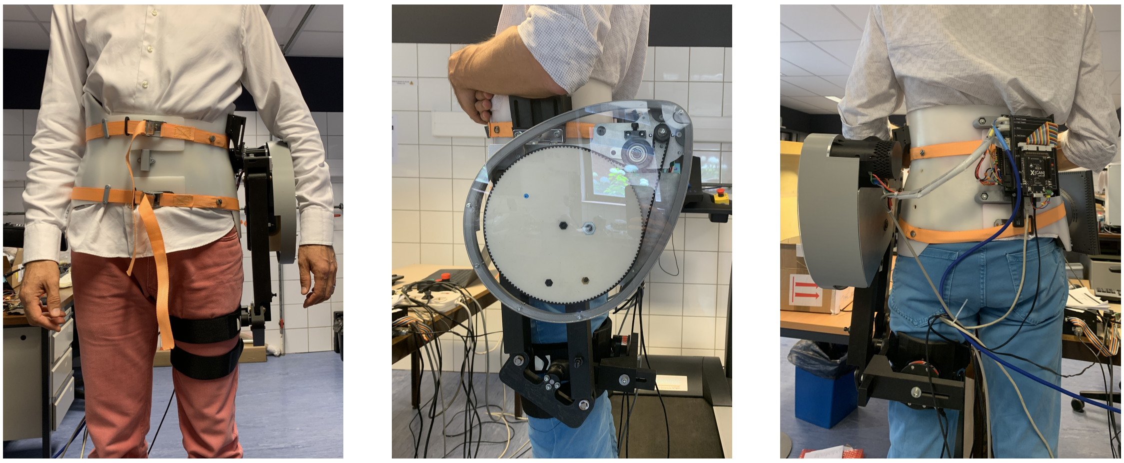

(a) Front view. (b) Side view. (c) Back view.

Figure 3.11: H.E.R.O. orthosis worn by the test subject, multiple views.

Weight of the prototype. The final weight of the device after alterations is $5.962[kg]$. The matter removed by the changes weights $0.56[kg]$ (total removed weight of $0.496[kg]$, after addition of the new support weight). Obviously, the majority of the weight comes from the transmission system and the electronics, which require bigger changes to lighten them. Table 3.2 gathers the weight of the main components of the orthosis.

EC60 flat (+ encoder)	350 g
EPOS2 70/10	330 g
myRIO	193 g
F/T sensor	475 g
Total	**1348 g**

Table 3.2: Main components weight.

3.2 Future improvements

The design of the H.E.R.O. orthosis, although currently functional, has its flaws, requiring to make some alterations in the future. This section summarizes the main issues met and suggestions of changes to be undertaken.

Spring management. As stated before, the spring's contribution to the force delivered is crucial to reach the goal torque. It does not obstruct the movement when walking but it hinders the sitting position or when climbing stairs. One should design a system to either disengage the spring once it reaches its neutral length or to place its anchoring point on rails which allows it to better align with the leg at higher flexion angles, not constraining the gap between the rods of the four-bar mechanism.

Thigh fastening system. Currently, the bottom of the four-bar mechanism is directly attached to the thigh of the subject thanks to two straps. However, due to the lack of freedom caused by this configuration, vertical parasitic forces are induced on the wearer's leg (see Section 5.1). A solution to get a more versatile setup is to put a rail at the end effector of the transmission system (i.e., the center of the bottom bar). This configuration would allow the sensor and the straps to stay still on the leg while sliding around the joint situated on the bottom rod, along with the flexion/extension movements.

Corset enhancement. The corset could be rethought to increase the user's comfort. Indeed, the whole device represents quite a weight that needs to be supported by its hips. Moreover, a helper is needed to put it on. A solution could be designed to improve its ergonomics and have a more practical device. Among other possibilities, a harness could be integrated to distribute the load and provide more autonomy to the subject. This alternative could also allow to shrink down the size of the corset to lighten it.

Another idea to explore is the removal of the adaptable fixations of the transmission mechanism on the corset. Their purpose is to adjust the four-bar system in height (displacement along the longitudinal axis) and its location with respect to the waist (displacement along the sagittal axis). Indeed, these pieces add weight that can be reduced if the mechanism is directly adjusted to its user or if one decides that the setting location is not that important.

Motor encapsulation. To prevent injuries due to the open outer rotor of the motor, a cover has been designed and 3D printed to isolate it. To avoid overheating, this cover was conceived to allow air to pass through. However, the piece produced still retains too much heat and the motor is at risk of overheating after extended uses. The screened cover should be improved with an expansion of the mesh. Figure 3.12 illustrates the current cover design and the possibility to further mesh it.

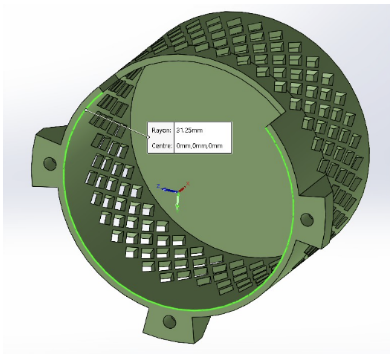

Figure 3.12: Motor screened cover CAD.

Weight and size optimisation. Lastly, the device weight should be investigated. It might be possible to downsize some equipment such as the sensor. A study could be carried out to reduce as much as possible the total weight, its distribution (maybe move the electronics further to the right by changing the cables), and the volume of the orthosis which limit the wearer's mobility around obstacles.

Chapter 4

Software design improvements

4.1 Middle-level controller design

The middlelevel controller's goal is to mimic the gait cycle. Locomotion can be described as a repetition of monophasic motor primitives [35]. The aim of this task is to design a framework able to reproduce various primitives. The gait being cyclical, the resulting primitive should be periodic with a frequency depending on the wearer's cadence and able to adapt when its walking speed increases or decreases. In this work, the cadence is learned using adaptive oscillators taking as an input the angular information provided by the motor's encoder.

4.1.1 Dynamic estimation of the walking cadence and phase

The force delivered by the H.E.R.O. orthosis to assist the patient needs to be coordinated with its gait cycle. This requires the controller to compute the walking state of the wearer at every time step and to be able to keep up with changes in its cadence. The solution designed in this project is an adaptation of Henri Laloyaux's work on the development of a bilateral active hip orthosis [35]. His solution uses adaptive oscillators to learn the cadence and phase from the hip angle. As his orthosis uses data from both the affected and sound legs, his calculations have been tailored for a unilateral device.

Adaptive oscillators (AOs) are tools used to dynamically filter a (possibly) noisy cyclical signal and learn its features such as the phase, frequency and amplitude. The signal is decomposed into a real-time Fourier series where N harmonics are kept for the estimate, one for each oscillator implemented in the solution. Their features are learned and an estimation of the input signal is obtained as a non-linear combination of the extracted variables. Finally, the error between the input signal and its reconstruction is computed and used as a feedback, driving the dynamic evolution of the state variables [30, 36]. A main advantage of this method is the estimated signal being, on average, phase-synchronized. Its delay-free attribute is a critical benefit from classic low-pass filtering approaches [37].

A schematic diagram of the AO system described in this section is displayed in Figure 4.1. Since typical hip angular profiles are quasi-sinusoidal, the number of AOs used in the implementation is set to N = 2 [35]. Indeed, this level of complexity already provides a reconstructed signal $\hat{\theta}(t)$ similar enough to the actual signal $\theta(t)$. The system state variables computed (i.e., the features) account for the phase φ, frequency ω and amplitude α. They are defined using an augmented phase oscillator in such a way that the phase resets when the input signal $\theta(t)$ reaches its maximum value, at maximum flexion:

$$\dot{\varphi}_i(t) = \omega i - \nu_{\varphi} \frac{F(t)}{\sum_{j=1}^{2} \alpha_j} \sin\left(\varphi_i(t)\right) \tag{4.1}$$

$$\dot{\omega}(t) = -\nu_{\omega} \frac{F(t)}{\sum_{i=1}^{2} \alpha_i} \sin\left(\varphi_1(t)\right) \tag{4.2}$$

$$\dot{\alpha}_i(t) = \eta F(t) \cos\left(\varphi_i(t)\right) \tag{4.3}$$

$$\dot{\alpha}_0(t) = \eta F(t) \tag{4.4}$$

where ν_{φ}, ν_{ω} and η are constant strictly positive gains determining the speed of phase synchronisation [36]. Laloyaux set them to 5.5 rad/s, 1.25 rad/s^2 and 0.5 s^{-1}, respectively [35]. A unique offset component is given by α_0 and the main phase of the sytem is given by the first AO with $\varphi \triangleq \varphi_1$.

The estimated signal $\hat{\theta}(t)$ is then defined as follows:

$$\hat{\theta}(t) = \sum_{i=1}^{2} \alpha_i(t) \cos\left(\varphi_i(t)\right) + \alpha_0(t) \tag{4.5}$$

The error signal $F(t)$ driving the dynamics of the state variables learning is the difference between the original and reconstructed signal:

$$F(t) = \theta(t) - \hat{\theta}(t) \tag{4.6}$$

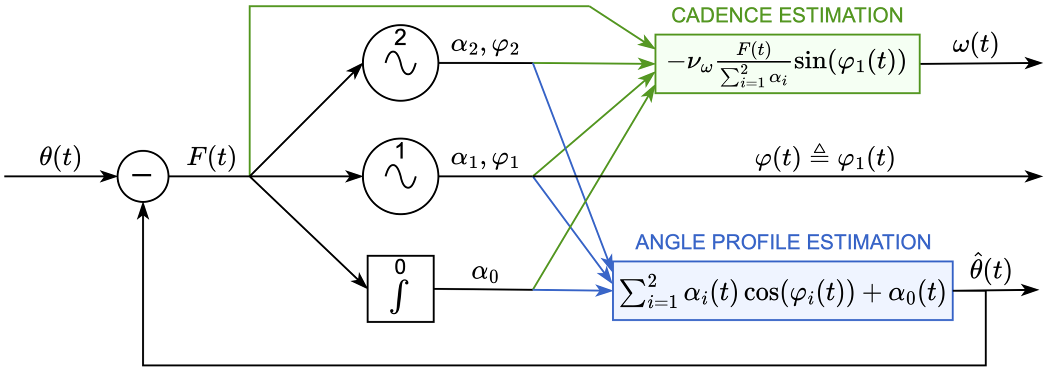

Figure 4.1: Block diagram of the AO system. A periodic input signal is decomposed into different harmonics. A pool of AOs is used to estimate the cadence of wearer, the phase and the angular profile (output signal). The error between the input and output signal drives the dynamics the state variables evolution. Adapted from [37].

4.1.2 Primitives definition

In order to have a maximum assistance during the swing phase of the gait and a minimum to null assistance when in stance phase, a repetition of periodic Gaussian-like primitives has been chosen as the force profile provided by the mid-level controller. As for the AO system, the design of the primitives is adapted from Henri Laloyaux' work [38].

The primitives are shaped by three features: their peak location μ, their peak width σ, their peak amplitude A and their peak duration L. They are defined using nested functions to avoid complex expressions.

Periodic peaks with a variable location. The first nested function f_μ uses a sinusoidal expression to generate a cyclical profile:

$$f_\mu(x,\mu) = \cos\Big(2\pi(x-\mu)\Big) - 1 \tag{4.7}$$

At the peak location $\mu \in [0,1]$, the function reaches a maximum of 0 and, at $(x-\mu) = 0.5$, its minimum value of -2 is reached. Indeed, the subtraction of 1 at the end of the formulae account for the shift in amplitude from $[-1,1]$ to $[-2,0]$. The presence of the μ parameter allows to move the signal over the phase x.

Monophasic shape: adjustable peak width and amplitude. The second function f_σ uses a Gaussian-like function with the function f_μ nested in it:

$$f_\sigma(x, \mu, \sigma) = e^{\frac{f_\mu(x,\mu)}{\sigma}} \tag{4.8}$$

where the parameter $\sigma \in]0, +\infty[$ is the primitive width. The value of f_σ is constrained in $]0, 1]$ and the peak shape gets narrower for a smaller σ whereas a bigger σ expands it, resulting in a flattened curve.

The remaining parameter of f_σ is the phase $x \in [0, 1]$. It is determined using the AO system previously explained and resets at the maximum flexion point of each cycle.

The resulting profile can then be multiplied by the amplitude factor A (i.e., the maximum force desired during a cycle). Therefore, by adjusting the three parameters μ, σ and A, complex primitives can be derived from a monophasic normalized Gaussian function.

However, the primitives as defined in Equation 4.8 provide a force profile constantly above zero since $f_\sigma \to 0$ when $x \to \pm\infty$, which contradicts the very definition of x. Preliminary experiments showed this behavior caused discomfort for the user as he had to fight against the residual force during the hip extension process. With this first definition of the force profile, the σ parameter had to be set at a low value as higher ones increased this phenomenon. The optimum value found by the wearer was $\sigma = 0.2$, with $\mu = 0.8$, which provides a short peak of force instead of an extended assistance for the whole flexion movement.

Figure 4.2 shows a recording of the force setpoint computed by the mid-level controller with regard to the hip angular position. This preliminary experiment used the primitives definition from Equation 4.8; the optimum parameters ($\mu = 0.8$ and $\sigma = 0.2$, for A = -20 at a speed of 2.5 km/h), have been determined by the user's sensations. As can be seen on the plot, to avoid fighting against the orthosis during the hip extension, only a small force could be applied before or after the flexion (i.e., at a level almost non-perceptible), hence the small σ value.

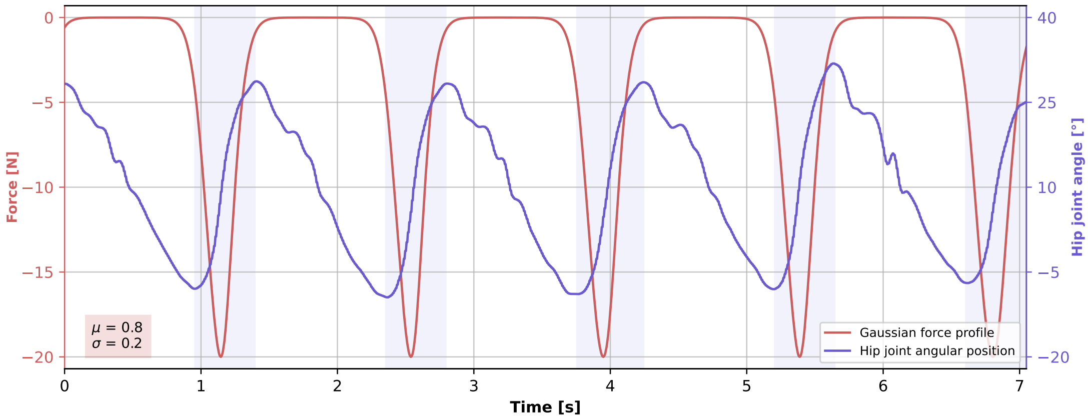

Figure 4.2: Recording of the force setpoint with regard to the hip angular position along time, produced by the first mid-level controller design. The flexion phases are highlighted. Walking speed = 2.5 km/h; $\mu = 0.8$; $\sigma = 0.2$; $A = -20$.

Adjustable section of force delivered. To counter this drawback, it has been decided to set to zero a fraction of the whole cycle. An extra parameter $L \in [0, 1]$ is introduced to the primitives' definition using another nested function f_L. It determines the length of the interval providing a force during a cycle:

$$f_L(x, \mu, \sigma, A, L) = \begin{cases} A \cdot \dfrac{f_\sigma - f_\sigma(x = \mu - \frac{L}{2})}{1 - f_\sigma(x = \mu - \frac{L}{2})} & \text{if } x \in]\mu - \frac{L}{2}, \mu + \frac{L}{2}[\\ 0 & \text{otherwise.} \end{cases} \tag{4.9}$$

The role of this function is to shift the whole profile obtained with f_σ such that the values at $x = \mu \pm \frac{L}{2}$ are null and to set to zero the force profile when the phase is outside of the wanted interval. Therefore, the values obtained when $x \in]\mu - \frac{L}{2}, \mu + \frac{L}{2}[$ are the only ones not being null. Lastly, a normalisation is applied and the result is multiplied by A to keep having a force profile with a peak height of the desired amplitude.

To reduce the number of parameters to adjust, it has been decided to set the L parameter equals to σ since the optimum primitives are obtained when the two parameters are closed to each other. Indeed, a large L combined with a small σ is irrelevant (the peak is too narrow for the L parameter to have an impact), same goes for the opposite scenario (for a small L, a large σ will produce a peak similar than with a smaller one).

Figure 4.3 shows the influence of the different parameters on their respective nested function and on the final force profile produced. The shifting action brought by f_L is well illustrated.

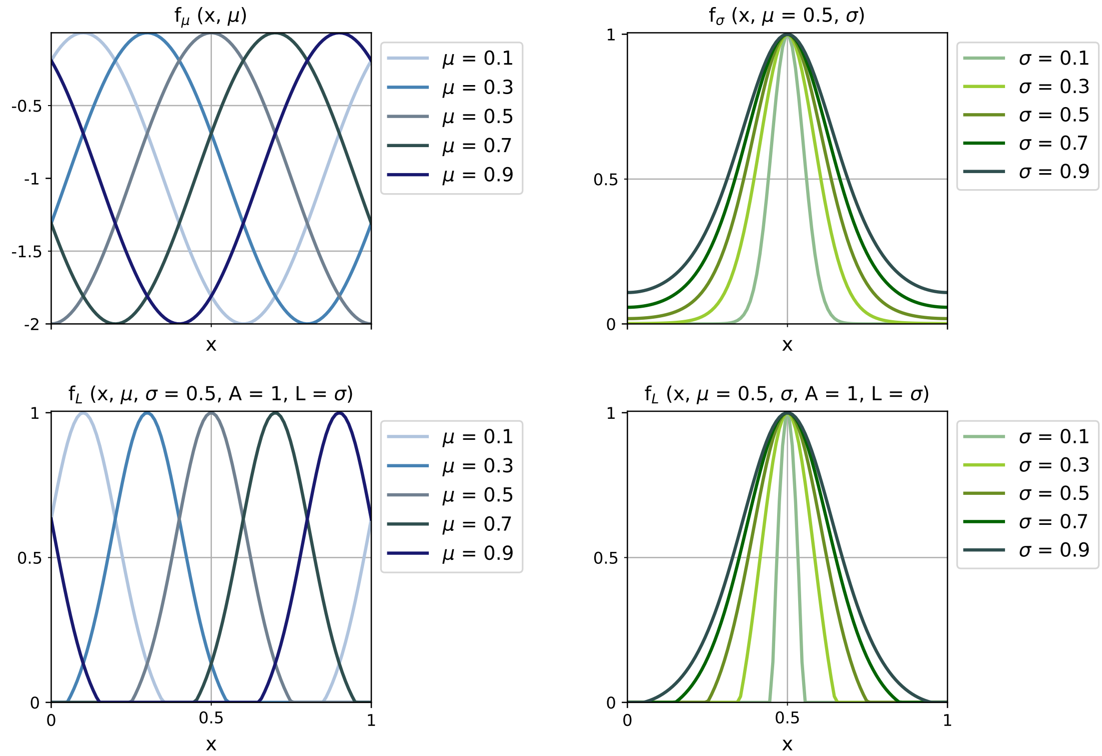

Figure 4.3: Influence of the μ and σ parameters on their respective nested functions and on the final primitives shape. Adapted from [38].

The new primitive definition allows for a larger σ value, providing a more extended assistance. Figure 4.4 displays recordings from the new design while keeping the same walking speed and peak amplitude A. The upper plot shows the force obtained with the previous optimum parameters (i.e., the same ones as for Figure 4.2); whereas, the second recording used the new optimum parameters. At 2.5 km/h, the σ value could be increased from 0.2 to 0.5 and the μ parameter was slightly changed from 0.8 to 0.75 which advanced the peak.

As can be observed, when keeping the previous values, the force produced do not cover the whole hip flexion phase and, therefore, no force persists during the extension. However, the new optimum force profile exceed the flexion phase and a small residual force remains at the beginning and end of the extension. Once again, this level of force is barely perceived by the wearer but allows for the force produced during the flexion to be of a good level for the whole phase. Finally, due to the change of the μ value, the peak location is moved up a bit.

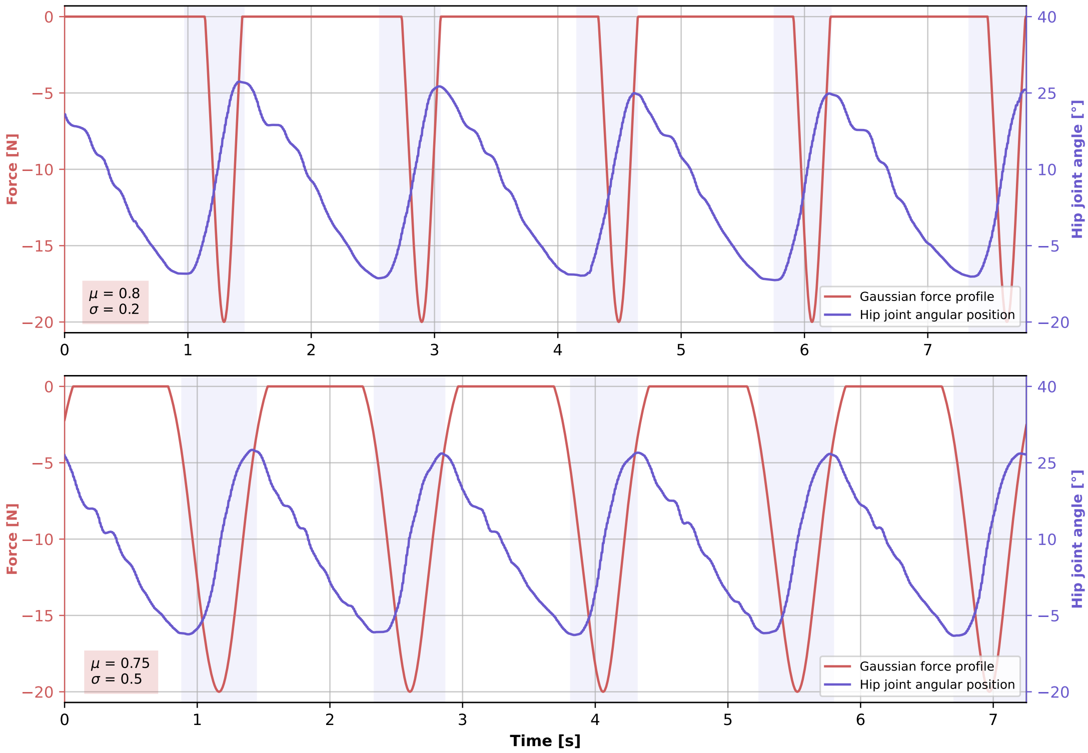

Figure 4.4: Recordings of the force setpoint with regard to the hip angular position along time, produced by the second mid-level controller design. The flexion phases are highlighted. Both graphs are at a walking speed of 2.5 km/h with $A = -20$. Upper (resp., lower) plot: $\mu = 0.8$ (resp., 0.75); $\sigma = 0.2$ (resp., 0.5).

4.2 LabVIEW implementation

As a reminder, Figure 4.5 shows the controller's LabVIEW program organization. Three main blocks are detailed in this work: the digital and analog inputs (see Appendix A), the low-level control and analog output (see Section 3.1.2), and the mid-level control. This last block has been one of the focuses of this year's work, while the two others are from previous works. As shown in Figure 4.5, this section is dedicated to the mid-level control implementation.

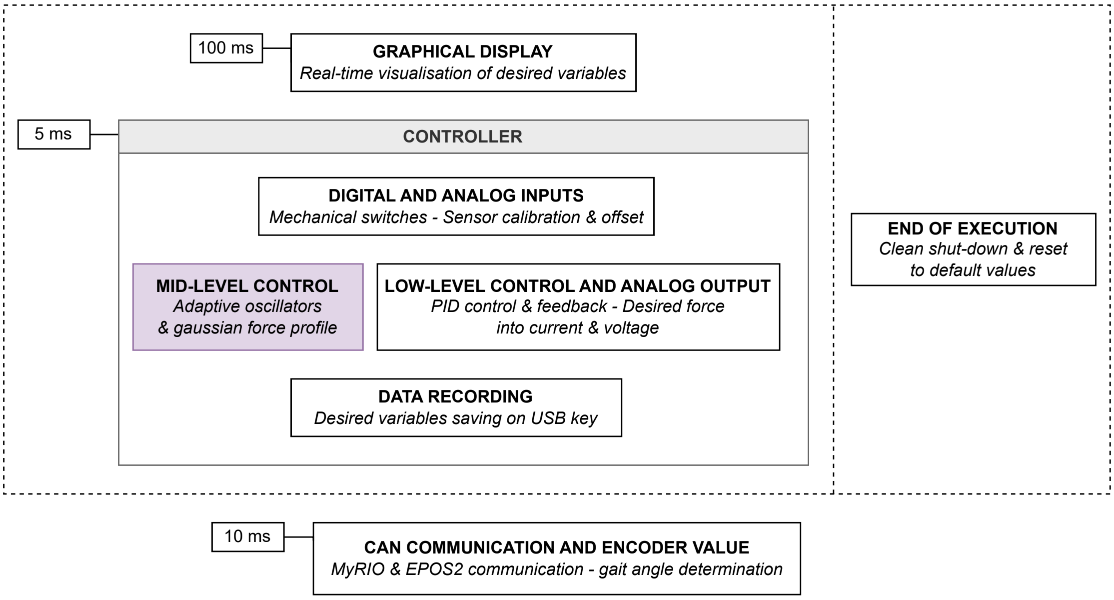

Figure 4.5: Overview of the LabVIEW implementation, highlight of the mid-level controller block.

4.2.1 Middle-level controller overview

The middle-level controller part of the LabVIEW program is divided into three steps described in Figure 4.6. The final output is a force setpoint sent to the low-level controller in order to be translated into the required current and voltage to be delivered. The main Virtual Instrument file (VI) of the orthosis' LabVIEW program uses sub-VIs to simplify its architecture; the description of the implementation keeps this substructure in order to have a accurate representation of the code.

First, the hip angle (acquired by comparing the motor displacements to the initial position) is used to determine the walking velocity of the wearer and its current state in the gait cycle (required for the next step). This is achieved by implementing two adaptive oscillators as developed previously. This step is detailed in Section 4.2.2.

Then, the information related to the gait retrieved by the oscillator system is integrated into the primitive equation defined earlier, along with the parameters adjusted by the supervisor. This step is detailed in Section 4.2.3.

Finally, the controller checks if the wearer is currently moving. This last part has been added due to issues with the oscillator system when the subject stopped walking. Indeed, it was taking too long to detect the halt and, therefore, force were still being delivered. This could end up knocking off the wearer, specially with hemiparetic patients. To limit the risk of injuries, it has been decided to deliver a force null if the hip angle remained still (within a range of ±3°, adjustable) during a certain time (currently set to 4 seconds).

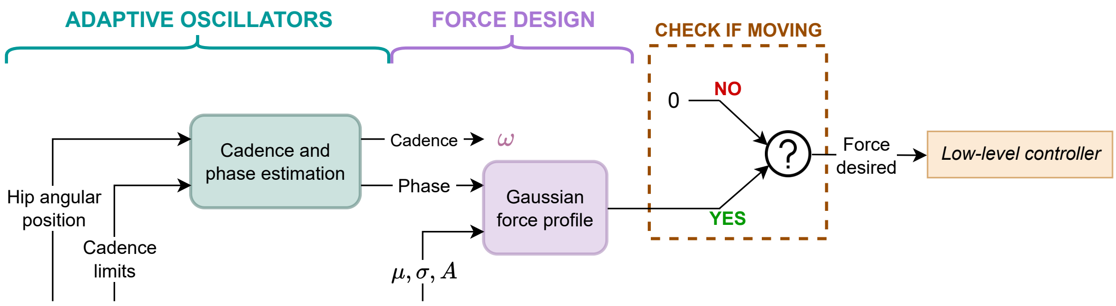

Figure 4.6: Overview of the mid-level controller implementation in LabVIEW, simplified structure.

The implementation of the AOs pool and primitives parts are based on VIs designed by Henri Laloyaux. The VIs developed in this project are adapted from his work.

4.2.2 Adaptive oscillators

The first part of the controller is about the detection of the gait cycle parameters. As said previously, a pool of AOs is implemented (two oscillators in this case), which allows to update the state variables at every time step. This solution requires to store the previous value of each variable since they are used in the definitions of the new values. Each variable is therefore saved for the next iteration in a feed-back node of LabVIEW (feed-back loops are in orange in the block diagrams). They are initialized to 2π for ω and 0 for φ_i, α_i and α_0.

The sub-VI "Cadence and phase estimation" from the main VI is represented in Figure 4.7. Once again, this VI contains two other sub-VIs to divide the code. This VI computes the error $F(t)$ between the reconstructed signal of the hip angular position $\hat{\theta}(t)$ and the actual hip angle $\theta(t)$. Equations 4.5 and 4.6 from Section 4.1.1 are used for the computations.

This comparison is at the origin of the state variables evolution. Indeed, the variables are then changed to reproduce as closely as possible the reel signal and decrease the error. The state variables update process is then split into the two sub-VIs, depicted in Figure 4.8. The outputs from these VIs are either used for the computation of another VI (i.e., for the next iteration), sent to the next step of the mid-level controller (i.e., the force profile) or displayed to monitor the experiments.

The last point of interest from Figure 4.7 is the cadence limits check part. Once again, this is an addition made to deal with the halt situation. Indeed, once the orthosis AOs system was stabilized after stopping, the resumption of the walk raised another issue. The resulting phase was sometime reversed or the controller had issue finding the good cadence. The main cause identified was the cadence variable ω sometime having a negative value. A solution for this problem, along with the halt detection explained before, was to never stop the AOs system. Indeed, since the force sent to the low-level controller is already set to zero after a short time, it does not matter if the cadence never reaches zero. It has therefore been decided to limit the gait angular frequency computed in a certain range delimited by a minimum and maximum values. With this solution, the cadence can never be negative and it reaches faster the new angular frequency when resuming walking. The maximum value is to prevent from any bugs where the cadence would reach impossible values. Currently, the limits are set to $2[\frac{rad}{s}]$ and $10[\frac{rad}{s}]$.

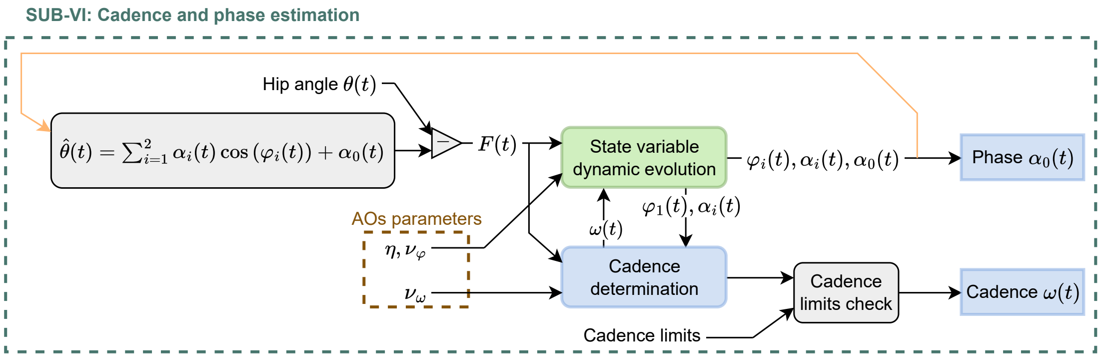

Figure 4.7: Zoom on the adaptive oscillators system of the mid-level controller implementation, simplified block diagram. Feed-back loops are represented by orange arrows.

Figure 4.8 focuses on the sub-VIs from Figure 4.7. The first one, "State variable dynamic evolution", is where the φ_i, α_i and α_0 variables are computed every iteration. The implementation uses Equations 4.1, 4.3 and 4.4 from Section 4.1.1. Once again, feed-back nodes were needed to store the previous value. Since the formulas give the derivative of the variables, the actual values are obtained by multiplying the derivative by the iteration period T (i.e., the time step) and adding the previous value.

The second sub-VI, named "Cadence determination", has the same role but for the ω variable with Equation 4.2. The purpose of this sub-VI was to lighten the program by computing the cadence apart from the other variables.

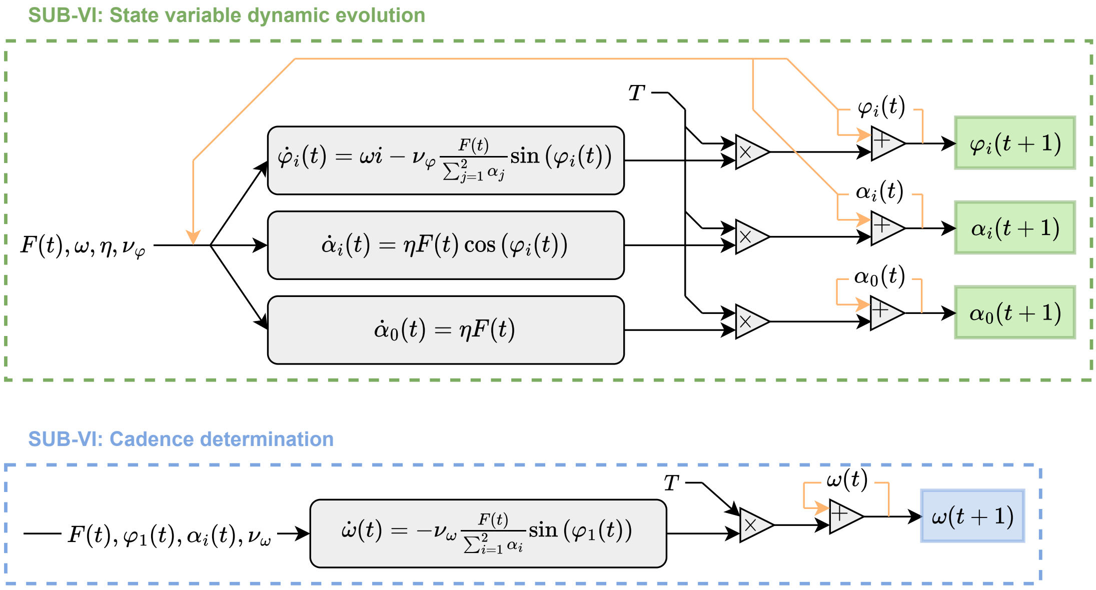

Figure 4.8: Zoom on the sub-VIs of the adaptive oscillators system from the mid-level controller implementation, simplified block diagram. Feed-back loops are represented by orange arrows

4.2.3 Gaussian force profile

The second part of the mid-level controlled is dedicated to the force instruction sent to the low-level block. Figure 4.9 shows the block diagram of the sub-VI "Gaussian force profile" from the main VI, and a subsequent sub-VI. The first one implements Equation 4.9 from Section 4.1.2. It takes as an input the current phase computed by the AOs system in order to get the value of the primitive at this point of the cycle. As a reminder, the optimum values are 0.75 for the peak location μ and 0.5 for the peak width σ and duration L (details about the settings process in Section 5.3). The amplitude factor A depends on the situation. A study has been made to determine the optimum force value with regard to the walking velocity of the test subject, the results can be found in Section 5.3.2.

Since Equation 4.9 (i.e., f_L) has the function from Equation 4.8 (i.e., f_σ) nested several times in it, a sub-VI has been created for f_σ with f_μ already integrated, simplifying the implementation.

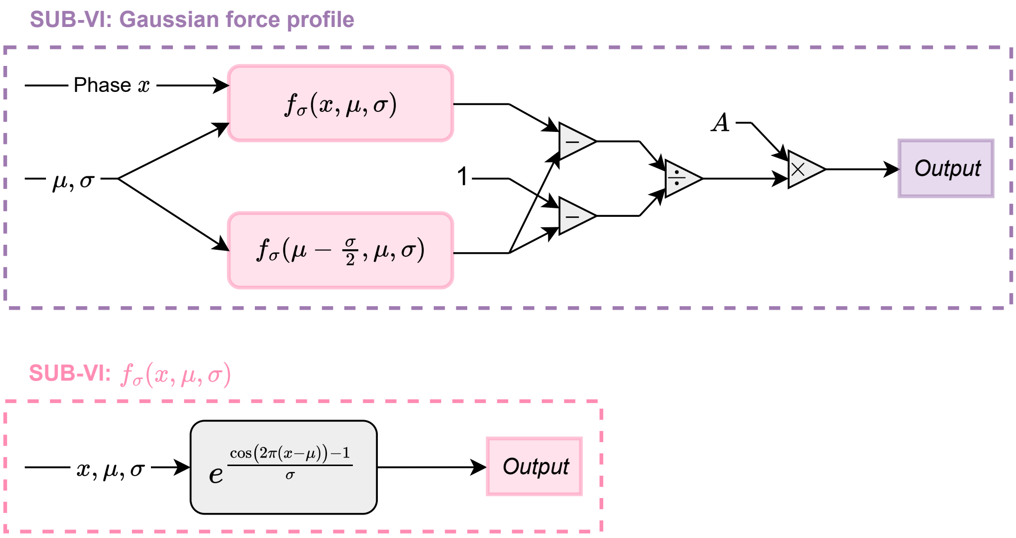

Figure 4.9: Zoom on the force design part of the mid-level controller implementation, simplified block diagram.

The final output of this step is the force to be delivered in case the subject is in motion. This force is sent to the low-level controller for its execution.

Chapter 5

Experimental performance assessment

This section summarises the different experiments done during this work and the relevant observations that could be made. Additional figures can be found in Appendix D.

5.1 Influences of the corset configuration

Goal. The four-bar mechanism and the transmission chain are attached to the corset using a hinge that can be moved horizontally along the sagittal axis and vertically along the vertical axis, see Figure 2.1 from Section 2.1 for the reference axes. This system allows to easily adjust the position of the mechanism. The objective aimed with this experiment is to study the effects of the various positions of the mechanism on the residual forces and the comfort of the user, with the ultimate goal of determining the optimum setting for the corset.

Methods. The vertical and frontal forces measured by the sensor (its x and y-directions) have been recorded while the subject walked on a treadmill at a speed of 3 km/h. The assistance was turned off and the orthosis only used in transparent mode, with no force setpoint. The mechanism was moved to various setting locations on the corset. To this end, nine settings have been determined by the combination of three vertical levels (low-middle-high) and three horizontal ones (front-center-rear); they are represented in Figure 5.1.

For the first part of the experiment, the nine configurations have been evaluated with the corset being positioned low on the wearer's waist. Indeed, the purpose was to bring down the center of rotation of the orthosis at the same level of the biological one, and this scenario required the corset to be set lower than usual with the mechanism placed at the lowest setting possible. The second part of this experiment have been achieved with the corset higher on the user's waist, at a more comfortable position.

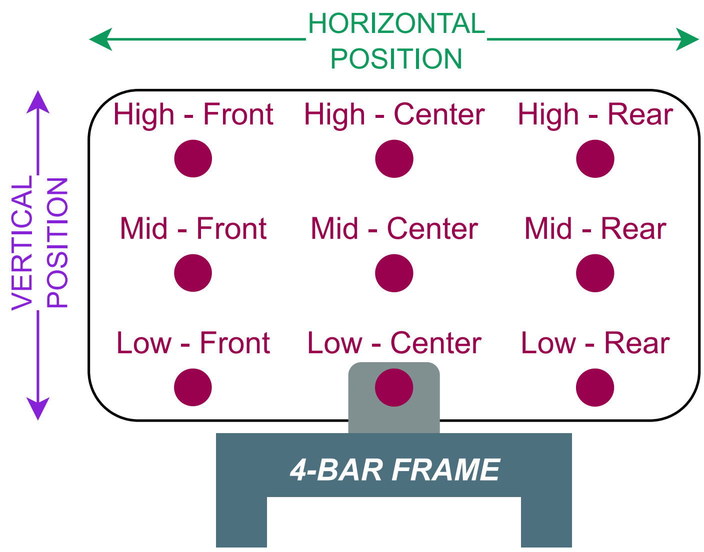

Figure 5.1: Corset different setting used for the experiment. The front of the orthosis is facing left, while its back is right.

Results: lowest position on the waist. The graphs of the vertical parasitic forces for the nine different configuration are shown in Figure 5.2. The horizontal displacements do not influence much the outcome. Indeed, no repeating pattern can be found by looking at the mean, maximum and minimum values computed in Table 5.1. Concerning the vertical setting, the higher one reduces the most the parasitic forces and therefore needs to be privileged.

The same study has been made with the y-directed forces (i.e., the frontal ones) and the graphs can be found in Figure D.1 in Appendix D. The reason these results are not displayed here is simply because they were less relevant as no pattern could be extracted. Moreover, reducing the frontal forces is less crucial than for vertical ones since the device do not constrain adduction/abduction movements, whereas upright motions of the leg are not possible.

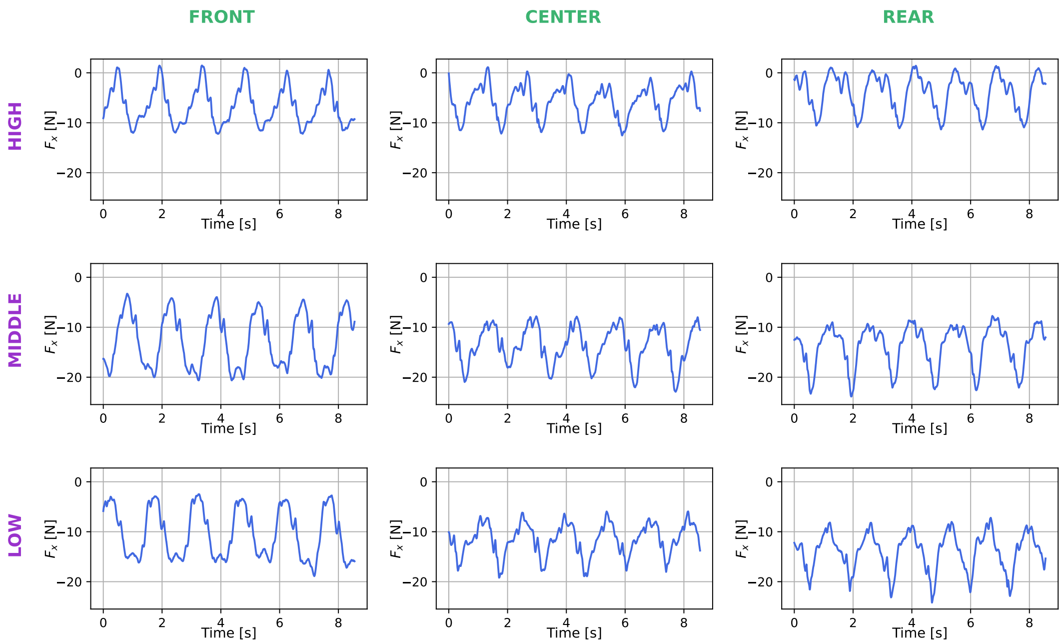

Figure 5.2: Vertical forces measured by the sensor while in transparent mode, at 3 km/h, lowest waist position. Multiple configurations of the corset are displayed.

	FRONT	CENTER	REAR	
Mean [N]	-6.6	-5.7	-4	**HIGH**
Max [N]	1.5	1.1	1.4	
Min [N]	-12.2	-12.6	-11.4	
Mean [N]	-12.7	-13.6	-13.8	**MIDDLE**
Max [N]	-3.3	-7.8	-7.7	
Min [N]	-20.7	-22.9	-23.9	
Mean [N]	-10.3	-11.6	-14	**LOW**
Max [N]	-2.5	-5.9	-7.2	
Min [N]	-18.9	-19.2	-24.2	

Table 5.1: Mean, maximum and minimum values of the nine configurations.

Results: higher position on the waist. Since the best setting was obtained with the highest level possible when the corset was low on the waist, it was determined that it did not matter whether or not the center of rotation of H.E.R.O. and hip were close to each other. The corset being less comfortable for the subject in that position, other configurations have been investigated to keep the transmission mechanism at the same level while adjusting the corset to a better height for the wearer. Indeed, the mechanism could not be anymore brought to an upper level due to the straps being already high up on the thigh. The new height necessitated to use the lower level setting of the corset to meet this requirement. The horizontal setting chosen was the front position as it seemed to be slightly better than the others, but the other positions would have been fine too.

The parasitic vertical forces of both the initially low corset position (with the highest level setting) and the new higher corset position (with the lowest level setting) are plotted in Figure 5.3. The new configuration increased the residual forces but was more comfortable for the wearer. However, he felt the orthosis pulling at the back of his leg when moving. The straps being fastened tight, another configuration was tested with the straps being loosened up a bit. This last configuration reduced the forces at more reasonable level while providing more comfort to the subject; it has therefore been decided to settle on this one as the best option for him.

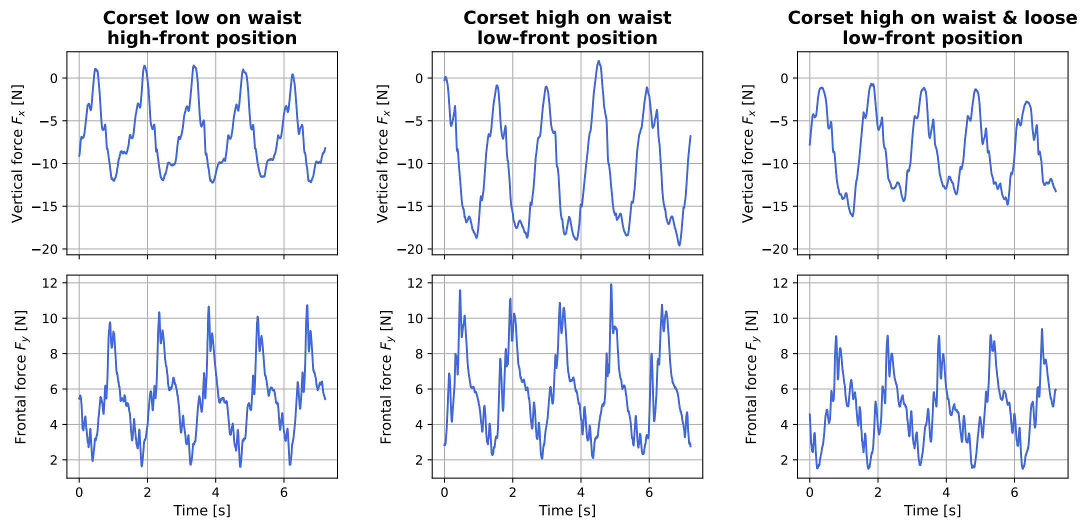

Figure 5.3: Vertical and frontal forces measured by the sensor in transparent mode, at 3 km/h. Three configurations are displayed.

Discussion. An optimum configuration has been determined for the corset with the low level and front settings while it is worn at a comfortable height for the user. The next experiments are achieved with this configuration and the height of the corset is set at the same level each time. The reference height chosen for the current subject is 116 cm from the ground to the top edge of the front of the corset; the center of rotation of the orthosis is about 5 cm higher than the estimated biological one. H.E.R.O. stays well in place with less than a centimeter of displacement from the start to the end of the experiments.

This experiment allowed to limit the vertical forces to a reasonable amplitude that do not bother the subject. To further decrease the parasitic vertical forces, one could install a rail system at the interface between the leg and the orthosis to reduce the friction.

A solution that could be engineered to make it even more comfortable and, more importantly, easier to put on alone is a harness system. This would also help with the weight distribution.

5.2 Controller's preliminary assessment

5.2.1 Transparent mode

Goal. Before assessing the proper functioning of the assistance, it was necessary to check if the orthosis can be transparent to the wearer (i.e., no assisting force). This experiment is important to limit the residual forces applied to the user's leg and to make sure the device do not hinder its mobility or cause resistance when walking. Moreover, the spring being required for high assisting forces, its addition to the H.E.R.O. orthosis should not impact the transparent mode.

Methods. The subject was asked to walk on a treadmill at a speed of 2.5 km/h. Although this speed is fast for hemiparetic patients, a sound subject cannot walk much slower without modifying its gait into an unnatural one. For the first part of the experiment, the spring was not mounted and the device had a zero force setpoint. It was added for the second phase, with still no assisting force. The hip angle, the force measured by the sensor and the current delivered are then retrieved to be analysed.

Results: hip angular position. As shown in Figure 5.4, the hip movements are smooth and regular. The range of motion without the parallel spring is about 28.6° (from -6.5° to 22.1°) and, when using the spring, the range is about 30.8° (from -7.1° to 23.7°).

Overall, the orthosis do not seem to hinder the subject mobility. The spring plot is similar to the one without it, although some slight irregularities can be noted. Indeed, the subject experienced a great fluidity of motion except for a sensation of steps with the spring. Nevertheless, he was not bothered by the orthosis itself but the weight added by the device made the walk more tiring than usual.

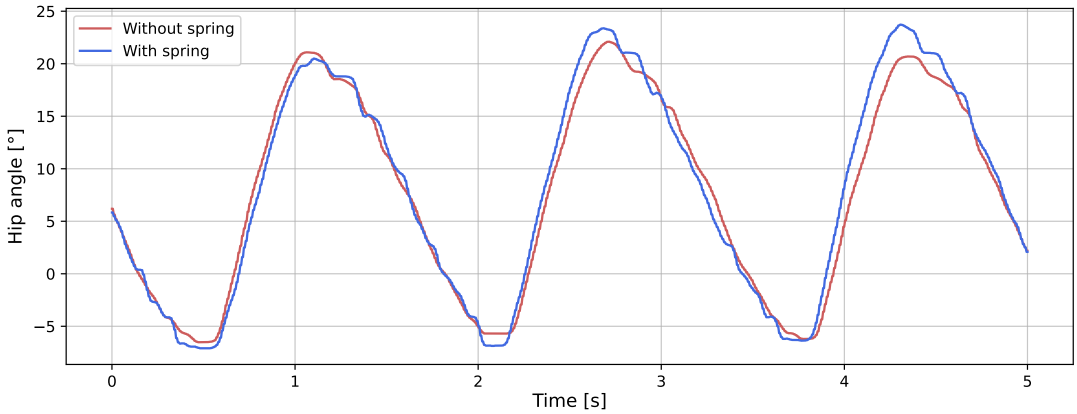

Figure 5.4: Hip angular displacement in transparent mode, with and without the parallel spring, at a walking speed of 2.5 km/h.

Results: force measured. The force measured by the sensor is plotted in Figure 5.5. This force accounts for the interactions in the sagittal plane (i.e., the direction for hip flexion/extension movements). The objective was to provide a zero force output and, from the wearer's perception, this goal has been met. He did not experience resistance or pushes from the orthosis. The recordings from the sensor back up these feelings as the mean force measured without the spring is -0.01 N, ranging from -2.5 N to 2.4 N. This level of force can hardly be perceived by the user. The residual force when using the spring is, as expected, slightly higher, ranging from -3.3 N to 4.4 N. Nevertheless, the mean value obtained is -0.008 N. The spring induces more fluctuations and higher peaks but it did not bother the subject though.

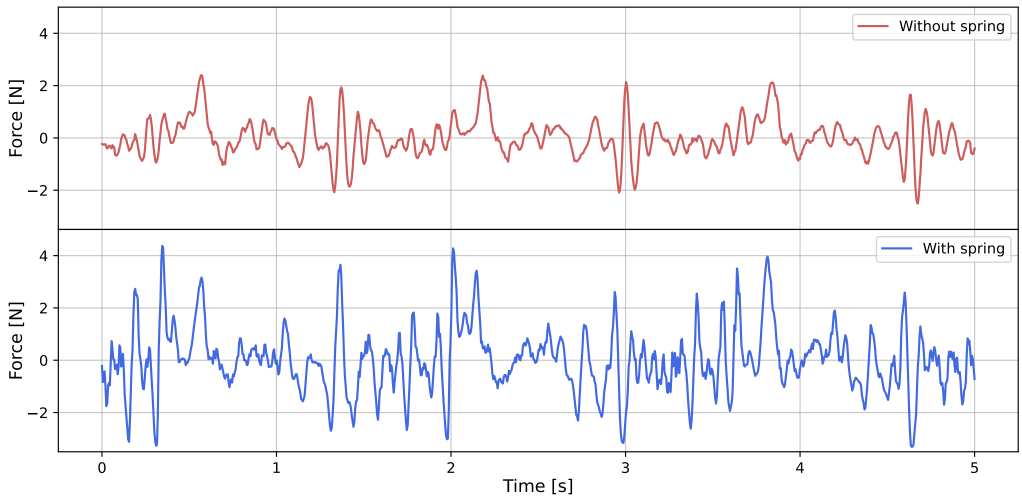

Figure 5.5: Force measured by the sensor in the sagittal direction in transparent mode, with and without the parallel spring, at a walking speed of 2.5 km/h.

Results: current delivery. Figure 5.6 represents the current setpoint computed by the low-level controller. The effect of the spring is well illustrated with a clear offset of the current. Indeed, when the H.E.R.O. orthosis is used without the parallel spring, the motor only has to counter the interaction forces due to the walk. However, when the spring is mounted, it has additionally to counteract the force produced by it. Since this force is directed the same way as the assisting force that the motor would have to produce (i.e., once the assistance is turned on), the device has to deliver a force in the opposite direction, hence the elevated positive current.

Obviously, the spring is useless in transparent mode since it becomes needed for high assisting forces. Nevertheless, it is important to ensure it does not hinder the transparent use of the orthosis. In addition, this experiment allows to assess the offset obtained. It can be observed that the current setpoint with the spring behaves similarly as when it is removed. However, its range is wider with a gap of 10.2 A (from around 9.3 A to 19.5 A), for 5.3 A without the spring (from -2.3 A to 3 A). This reflects the action required by the motor to counter the force and can be linked to the higher force peaks measured by the sensor. The overall offset is about 13 A, with mean values of 13.4 A and 0.4 A, with and without the spring respectively.

The use of the spring however brought an issue regarding the current saturation. Indeed, the levels reached by the current were sometimes out of bound as the maximum value is set to 20 A. Due to the lack of a current overflow management system, once the current setpoint reached the saturation level, it sticks at this value with a PID error constantly growing since the motor is not able to deliver what the low-level computes. The only way to bring it back to a proper value was to reset the PID controller. This issue should be remedied in a future work with the addition of a management system for such situations or design modifications preventing it from occurring.

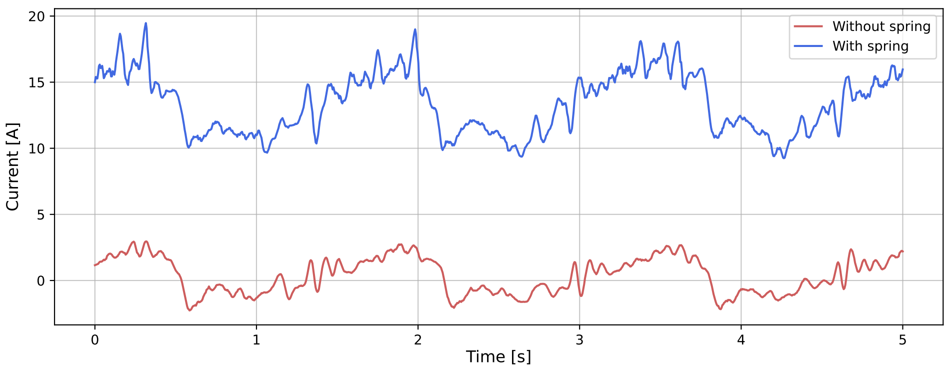

Figure 5.6: Current delivered in transparent mode, with and without the parallel spring, at a walking speed of 2.5 km/h.

Discussion. This experiment allowed to attest the proper functioning of the transparent mode of the H.E.R.O. orthosis. Its use do not hinder the subject's mobility and the controller reacts properly to its movements so minimum forces are produced on its leg. It also allowed to check the new values determined for the PID gains: the controller adapts quickly to changes and its use is smooth. The values still need to be confirmed when the assistance is turned on, of course.

The use of the parallel spring is overall well handled by the controller except for the saturation issues pointed out and the steps being perceived. However, the current overflow does not represent an issue when the assistance is activated since the motor does not need to (fully) counter the spring action anymore.

The steps could be due to three causes. One: the current controller from the EPOS experiences some jumps and difficulties to correctly regulate the motor since the current demanded with the spring in transparent mode is generally higher than its nominal current. Two: the jumps may come from the power supply since it reaches its limits too. Three: the last hypothesis is that they come from the motor steps generated by the rotation between its poles, introducing a cogging torque amplified when greater efforts are asked to the motor [39].

5.2.2 Middle-level controller

Goal. This section investigates the proper functioning of the mid-level controller implemented during this work. As a reminder, it is divided into two stages: first the AOs pool to determine the phase of the system, then the identification of the appropriate force setpoint. The orthosis limits are also looked into and compared to the initial goal of $10.2[Nm]$ (corresponding to a force of $36.4[N]$).

Methods. The first part of this experiment aims at assessing the AOs system by alternating walking speeds. Using a treadmill, the subject was asked to walk at a velocity of 2.5 km/h and then to speed up to 4 km/h to determine the adaptation time of the oscillators. Next, the halt and the initiation of motion situations have been simulated by reducing the speed from 2.5 km/h to zero before resuming walking at 2.5 km/h.

The second part investigates the force profile delivered with the effects of the three adjustable parameters (μ, σ and A) being studied separately. The peak location μ was first set at 0.4 and then set to 0.75 to evaluate the effect on the stride when walking at a speed of 3.5 km/h. As for the peak width σ (and section of force delivered), its influence on the final shape of the force measured by the sensor has been studied by comparing two conditions: $\sigma = 0.2$ and $\sigma = 0.5$ at 2.5 km/h. Finally, the peak amplitude A was increased until a current saturation was reached, with and without the parallel spring, to determine the limits of the device. This last part was achieved at a speed of 2 km/h when the spring was removed, and 4.5 km/h when used. This choice is due to the influence of the speed on the force impact; a small force will not be well perceived at a high speed, whereas a larger force risks destabilizing the wearer at a low speed.

Results: adaptive oscillators. Figure 5.7 displays the ability of the controller to adapt its output in case of a sudden change of speed. The device keeps up well with the user's cadence since one cycle is required to adapt the phase; in other words, after about 1.2 seconds, the force delivery is synchronised again. From the wearer's perspective, the adaptation is felt as instantaneous and smooth.

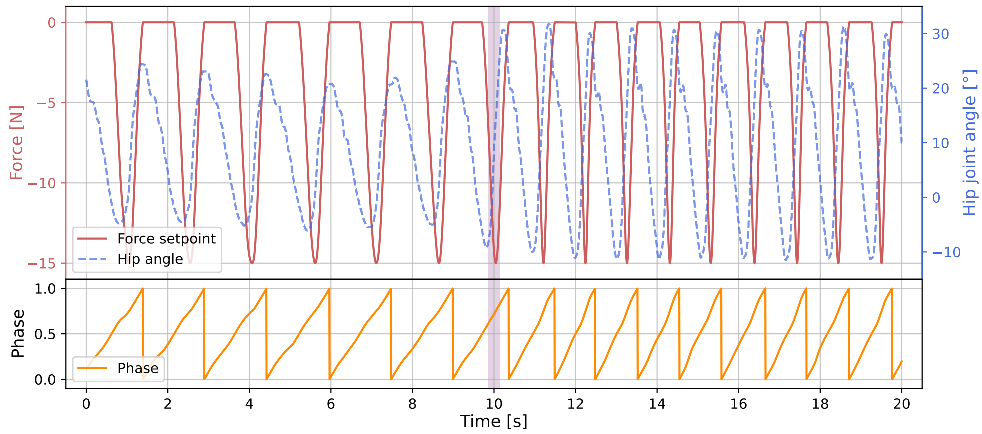

Figure 5.7: Increase of the walking velocity from 2.5 km/h to 4 km/h. The change in speed is highlighted by the vertical bar.

Next is the halt condition. The device behavior is illustrated in Figure 5.8 where the treadmill speed is reduced to zero. As a reminder, the controller has a time interval set to 4 seconds to stop delivering force after an absence of motion has been detected. The recordings plotted indicates a delay of 6 seconds before the interruption of the assistance. This delay may be dangerous when worn by a patient as a few impulses are delivered on the wearer's leg which could knock off the person.

This long stopping time could be due to the delays of the treadmill. Indeed, for safety precautions, the halt condition is not immediate and takes about 1 to 2 seconds to be achieved. Given the implementation of the halt detection of the controller, this stopping is a time process during which the 4 seconds interval is not activated. Additionally, the parameters of this detection system may be incorrectly set, or the system may need to be redesigned for a more efficient one.

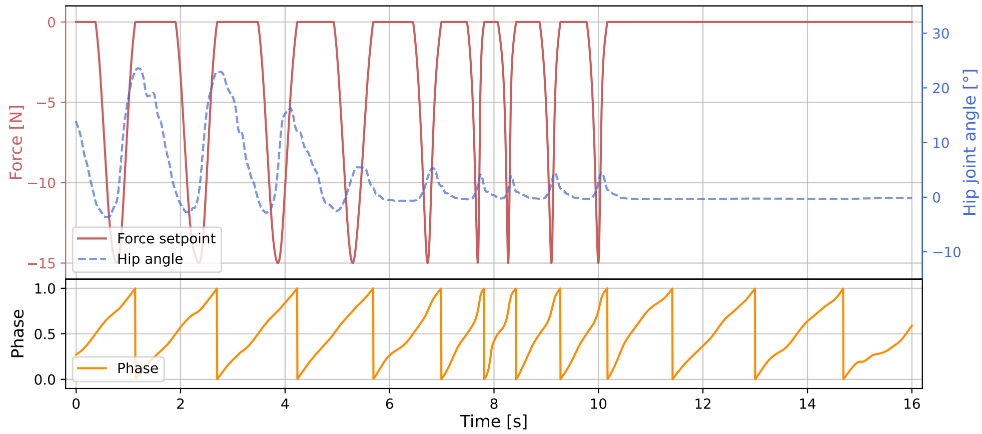

Figure 5.8: Detection of the halt from 2.5 km/h.

The last situation studied concerns the motion initiation. As explained in Section 4.2.2, the oscillators of the mid-level controller are never stopped and are bound by a minimum angular frequency. The force setpoint sent to the low-level controller is set to zero while no change in the hip angular position is detected which allows the AOs pool to keep functioning at a certain cadence and stay ready for walk resumption. The synchronization of H.E.R.O. is therefore almost immediate with again only one cycle needed to be in-phase (about 1 second). From the wearer's point of view, the transition appears smooth and efficient.

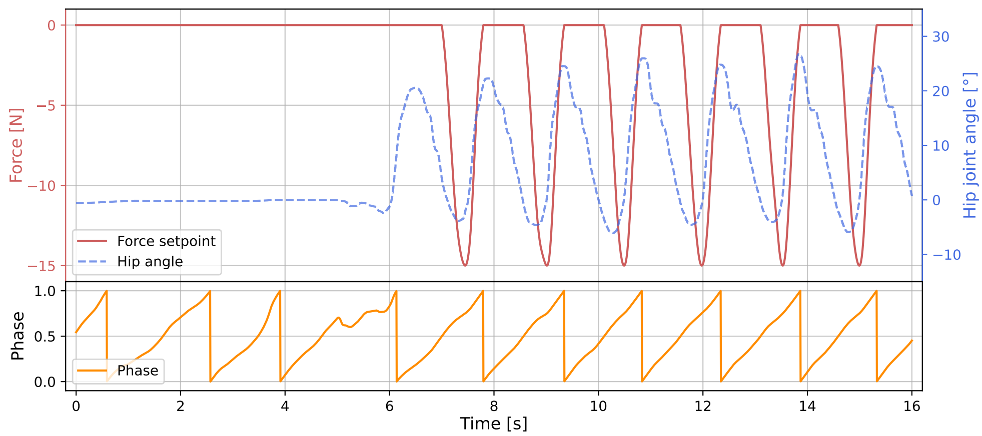

Figure 5.9: Adaptation of the mid-level controller when resuming the walk at a speed of 2.5 km/h.

Results: force profile design. The first parameter analysed is the peak location μ with the graphs from Figure 5.10. The shift between the two conditions can clearly by observed. The second plot, with $\mu = 0.75$, represents the optimum value of the parameter, whereas the first one, with $\mu = 0.4$, is a very uncomfortable setting for the user who has to fight against the orthosis during the extension stage of the cycle.

The difference between a well and poorly adjusted parameter can be seen with the deformation of the hip angular movement. Indeed, with an improper setting, the stride is shortened and the curve appears flatter. On the other hand, with the optimum setting, the stride is enhanced and the propulsion from the assistance allows wider movements. The subject expressed a great sensibility to the variations of the parameter, with a threshold of 0.05 to detect a change. It is therefore of great importance to adjust it correctly. A study on the matter is described later on in Section 5.3.1.

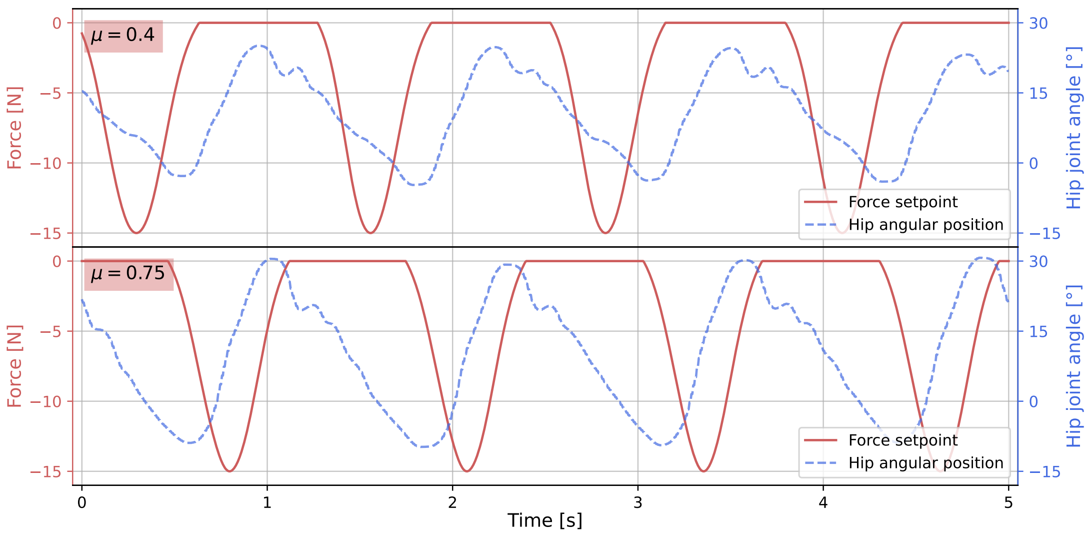

Figure 5.10: Peak location variation from $\mu = 0.4$ to $\mu = 0.75$, at a speed of 3.5 km/h.

Figure 5.11 shows the force measured compared to the force setpoint with two different σ values. The first one is too small, resulting in a very narrow peak. The force is delivered for a short period of time and in the form of an impulse. This situation is uncomfortable for the user who do not get a proper assistance for the whole flexion movement. However, once the proper value for σ is found (the second plot), the user's sensation was a great assisting force all along the flexion and no too steep increase of the force.

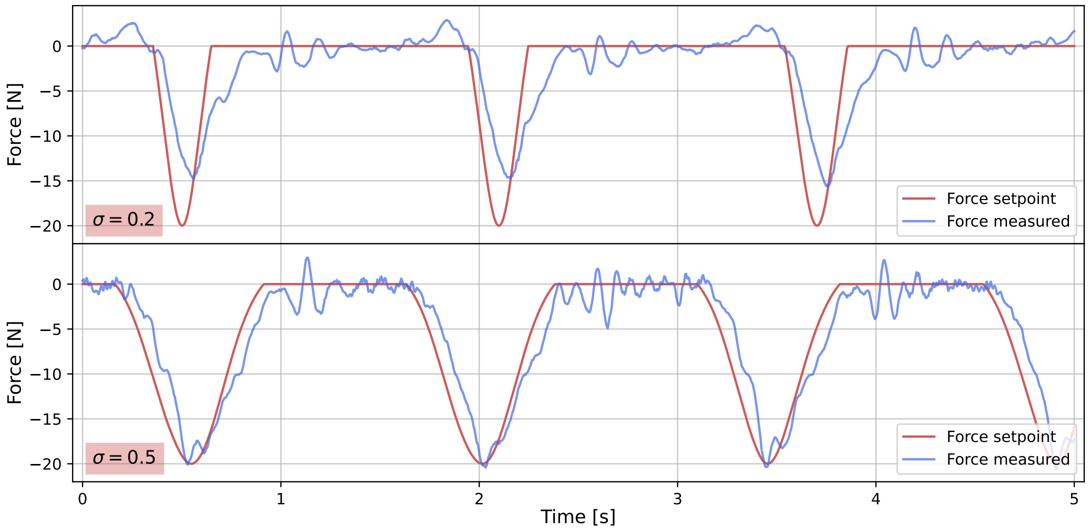

Figure 5.11: Peak width variation from $\sigma = 0.2$ to $\sigma = 0.5$, at a speed of 2.5 km/h.

The last parameter of interest is the peak amplitude A. Its limits due to a saturation of the current being delivered are shown in Figure 5.12. Obviously, the maximum value depends on whether or not the spring is mounted. The first graph accounts for the situation where it is not and the limit is reach for a force setpoint with $A = -30$ N. Yet, the force measured and therefore the real force delivered by the H.E.R.O. orthosis do not reach this aimed level with a maximum of about 24.5 N.

Regarding the second plot, with the use of the parallel spring, the force setpoint that could be reach before an overflow of the current is $A = -38$ N. The maximum value reached by the force measured is at about -35.5 N, close to the initial goal set to 36.4 N. The small gap between the values obtained with and without the spring are due to the different speeds. Indeed, a high speed requires more current to quickly execute the aimed task, which would almost immediately saturate without the spring. The graphs attest of the importance of the spring to be able to assist at a higher pace and amplitude. The lack of efficiency illustrated by the force measured being lower than expected suggests that the PID gains may not be perfectly tuned. However, no better gains could be determined manually. Another explanation comes from losses in the transmission chain.

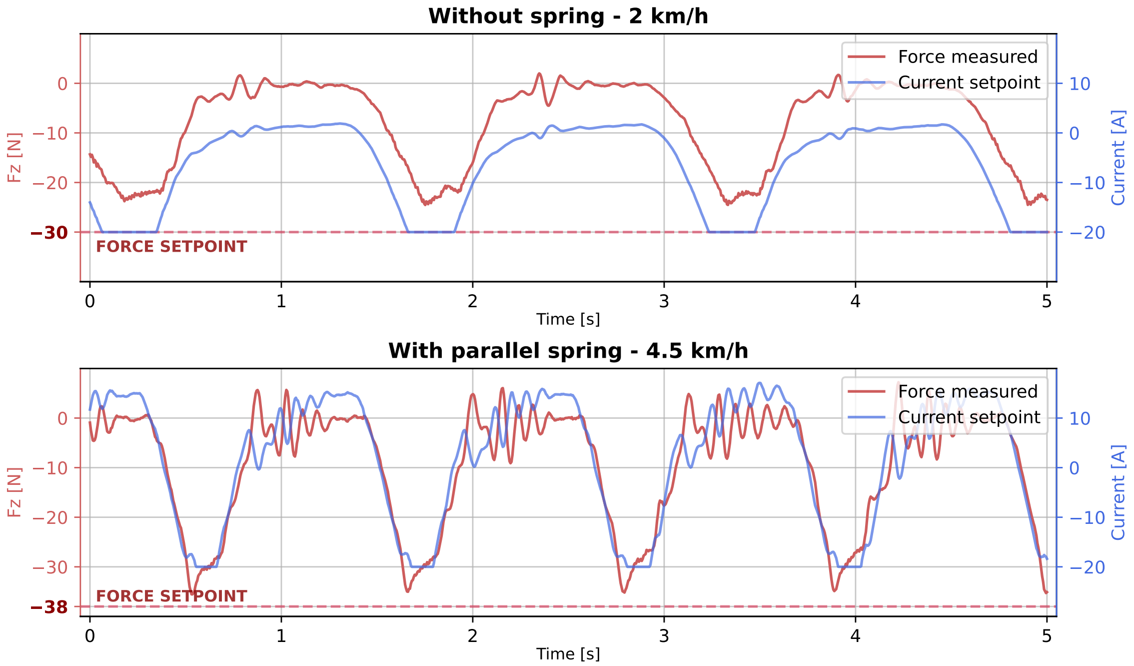

Figure 5.12: Force measured and current setpoint, with and without the use of the parallel spring.

Discussion. Overall, the mid-level controller implemented in this work proved to be efficient to regulate the action of the device according to the wearer's pace and needs. The reaction time when beginning to walk or changing speed lasts about one second and is perceived as (almost) immediate to the user. The force profile delivered can easily be modulated to fit the user's requirements and improve its comfort. The goal of providing a smooth and adequate assistance has been achieved.

Although the results attest of its proper functioning, some flaws should be looked into in a future work. The delay for the halt detection raises an issue and requires improvements. Likewise, the device seems to face difficulties to deliver the right amount of force. The issue may come from the PID gains or losses in the transmission chain. Nevertheless, the force measured is still very close to the setpoint; the performance of H.E.R.O. regarding the force delivery can therefore be qualified as fulfilling its goal, with an acceptable efficiency gap

5.2.3 Effect of the parallel spring

Goal. As previously demonstrated, the spring is of a great importance when delivering high assisting forces. Even though it has already been partly characterised in prior experiments, this study aims at better analysing its behavior and the influence it has on the orthosis efficiency.

Methods. Since a preliminary assessment of the spring has already been conducted in transparent mode, the assistance was turned on during this experiment. An assisting force of -10 N was asked of the device when the subject walked on a treadmill at a speed of 2.5 km/h. Reference data has been collected when the spring was removed. The spring was then mounted and the force measured by the sensor as well as the current setpoint have been recorded.

Results. The offset of the current brought by the spring is well illustrated in Figure 5.13. As a reminder, the offset determined in transparent mode was 13 A. The two graphs plotted are similar and follow the same curve but at different levels. The offset during this experiment is of 11.5 A with a mean value at -2 A for no spring curve and 9.5 with it. The offset is not constant and decreases with the force targeted, possibly due to losses in the transmission process. The ranges of current are similar too with an interval of 11.4 A for the no spring curve (from -8.7 A to 2.7 A) and 12 A for the other one (from 3.2 A to 15.2 A).

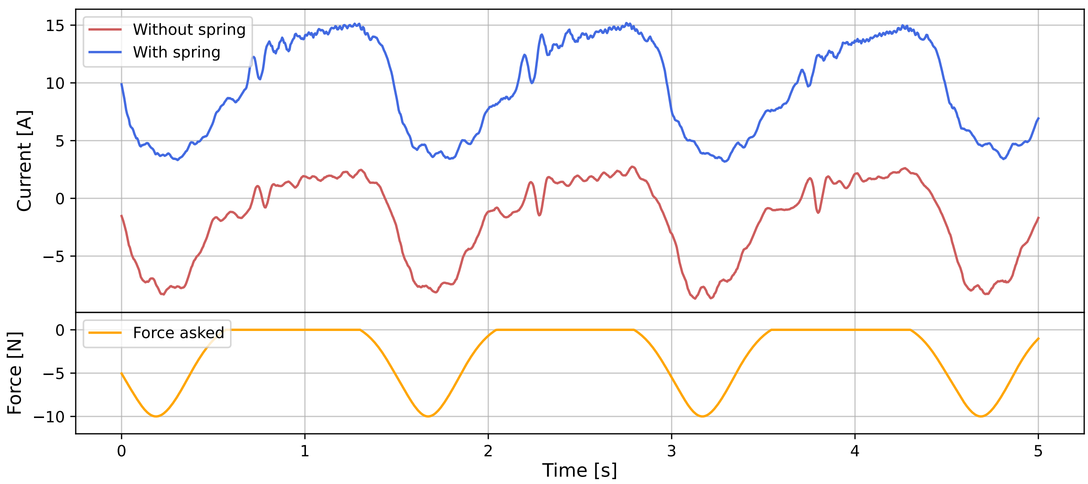

Figure 5.13: Current setpoint of the orthosis for a force setpoint of -10 N at 2.5 km/h, with and without the parallel spring.

The two situations also have similar curves for the force measured, as shown in Figure 5.14. Although, in transparent mode, the parallel spring induced more instability than without it, this is not the case anymore as both equally fluctuate.

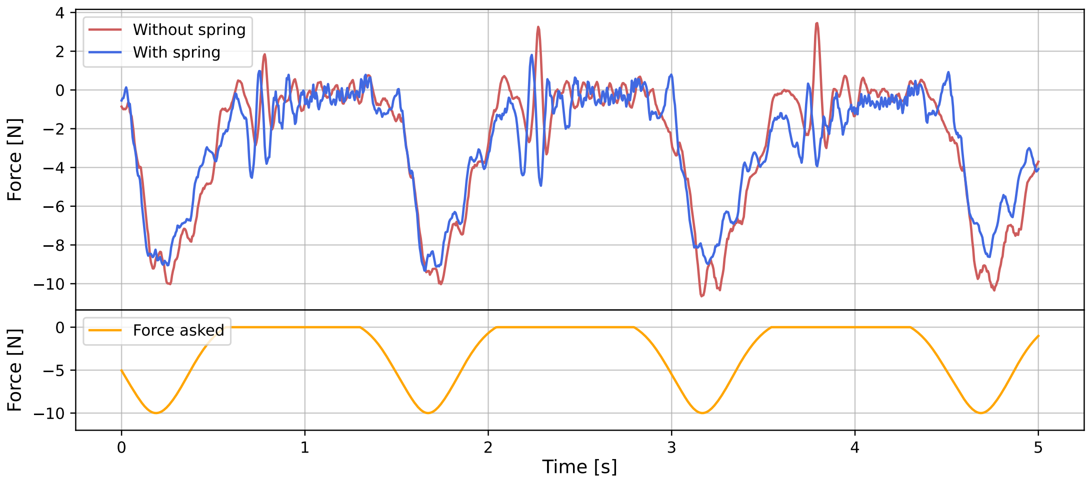

Figure 5.14: Force measured by the sensor for a setpoint of -10 N at 2.5 km/h, with and without the parallel spring.

Discussion. When used in a situation where an assistance is provided to the subject, the spring effects are very beneficial. Indeed, the force delivered behaves the same way as when it is not mounted but with the current being offset, giving a larger range of current for the controller. Higher forces can be achieved so the device can adequately assist the user, even at high velocities.

Other than the current saturation issue observed in transparent mode, the spring fulfills its purpose to provide an additional force to the wearer's leg during the flexion movement.

5.3 Settings optimisation for the mid-level controller

5.3.1 Optimum peak location and width

Goal. The performances of the mid-level controller being assessed, it is now time to optimise the parameters. This study focuses on determining the optimum peak location μ and width σ. Indeed, their importance having been established in previous experiments, it makes sense to find the best ones for the subject. To add another dimension to this experiment, it has been decided to use psychophysics for the protocol as it has (almost) never been done in bio-robotics.

Psychophysics studies the sensory system behavioral response to a physical stimuli [40]. In other words, it is a branch of psychology that aims at quantifying the relationship between a sensory stimuli and the psychological perceptions and sensations it evokes.

Methods. The peak width σ was first determined by trial as this parameter's effects were easily perceived by the subject. A psychophysical test was therefore not required and the optimum value could simply be established by increasing it until the subject determines it is not too narrow nor too wide, saving some times. As for the other parameter, the peak location μ, it is more subtle; a psychophysical protocol has therefore been chosen for its assessment.

Psychophysical experiments are usually designed for large groups of subjects with the goal of determining the thresholds at which individuals can detect differences in stimuli and the relationship between the physical properties of the stimuli, and the psychological responses elicited. It is widely used in preference studies to analyse the importance of certain factors regarding a product. As the experiments conducted in this work only had one subject, many psychophysical experimental protocols are not applicable in this case. However, a study has been carried out by Amlani and Schafer [41] to determine the optimum settings for a hearing aid for individuals using the paired-comparison procedure from psychophysics. The protocol followed in this experiment takes inspiration from theirs.

The first step for a paired-comparison study is to determine the threshold at which a variation of stimuli is perceived [42]. To this end, the peak location μ parameter was first slightly modified by a small value step. A pair of two settings were then presented to the subject with a control value for one and either the new slightly different value or the same control parameter for the other. He was asked to determine whether or not a change occurred. The step was gradually increased until the subject could tell without making any mistakes. Finally, the threshold was double-checked by modifying the control value in both directions (i.e., decreasing and increasing it).

Once the threshold had been determined, a tournament procedure could be conducted. Different kinds of tournament procedures can be found in the literature but the adaptive Round-Robin tournament best suited the experiment. A classical Round-Robin tournament consists of a pairwise testing of every pair of possible values. With n being the number of settings, the number of pairs to be tested p

can be computed using Equation 5.1. If the number of setting values is large, the number of pairs to be evaluated with the method would be too much. Besides, it goes without saying that many values could be quickly disqualified by the user. The Round-Robin tournament provides an alternative with its adaptive derivative. This time, a larger threshold is first used over the whole range of values to roughly select the values of interest within less pairs by having the subject select its preferred value for each couple. A next round is then carried out with a refined threshold on a reduced group of settings chosen to be centered on the winning value from the previous round. And so on, until the threshold is refined to the original one.

$$p = \frac{n(n-1)}{2} \tag{5.1}$$

The experiment was conducted two times: the first time was before the changes made to the primitives definition, and then it was redone with the new definition (i.e., with the addition of the L parameter).

Results: threshold determination. The threshold regarding the peak location μ, obtained by trial, is 0.05. Given the $]0,1]$ range of values, 20 settings would have to be tested with the classical Round-Robin tournament, for a total of 190 comparisons with Equation 5.1. With the adaptive version (chosen for the experiment), a first round is designed with a threshold of 0.2, giving 5 settings and 10 pairwise comparisons. A second round is carried out with a threshold of 0.1 within an interval of ± 0.2 around the winning value from the previous round, giving a total of 5 settings too. Lastly, the final round is conducted with the original threshold of 0.05 within an interval of ± 0.1 around the winning setting of round two which, once again, gives 5 setting values and 10 pairs. A total of 30 pairwise comparisons are therefore required for the adaptive Round-Robin tournament, instead of the 190 ones needed with the classical version.

Results: first version of the primitives definition. Only the results of this first experiment are summarized here, the details can be found in Appendix D with Tables D.1, D.2 and D.3, and with Figure D.4. First, the peak width σ was set to 0.2 after a trial test. The psychophysical experiment was then carried out to determine the peak location μ. The winning setting from the tournament is $\mu = 0.8$.

Results: final version of the primitives definition. The same protocol was applied to the new primitives function. This time, the peak width that best suited the subject is $\sigma = 0.5$.

The Round-Robin tournament results are transcribed in Tables 5.2, 5.3 and 5.4. Each row computes the wins of the corresponding μ values with regard to the other values (arranged in columns), whereas each column counts the defeats of the corresponding value. In other words, a 1 occurring in a row means that the μ value from the row won against the corresponding value from the column, and a 0 is the opposite scenario.

The first round immediately redirected the search around $\mu = 0.6$. By refining the result with two more round, the final optimum value determined is $\mu = 0.75$. The whole process is illustrated in Figure 5.15. This graph represents the result as winning percentage with cumulative results obtained by arranging the results for the second or third round within the y-axis range determined in the previous round for the values reported in the said round. As can be seen in the tables and in the graph, choosing between two values can sometimes be difficult for the subject. Indeed, in the first and third round, $\mu = 0.6$ won over $\mu = 0.8$ but not in the second round. The reason is that one was a bit too early while the other one was slightly too late and the user had to decide which one impaired most its walk.

μ values	0.2	0.4	0.6	0.8	1.0	**WINS**
0.2	\	0	0	0	0	0
0.4	1	\	0	0	1	2
0.6	1	1	\	1	1	**4**
0.8	1	1	0	\	1	3
1.0	1	0	0	0	\	1
LOSSES	4	2	**0**	1	3	**10**

Table 5.2: First round of the adaptive Round-Robin tournament, final version. Threshold of 0.2 and range of $]0, 1.0]$.

μ values	0.4	0.5	0.6	0.7	0.8	**WINS**
0.4	\	0	0	0	0	0
0.5	1	\	0	0	0	1
0.6	1	1	\	0	0	2
0.7	1	1	1	\	1	**4**
0.8	1	1	1	0	\	3
LOSSES	4	3	2	**0**	1	**10**

Table 5.3: Second round of the adaptive Round-Robin tournament, final version. Threshold of 0.1, centered on 0.6 and range of $[0.4, 0.8]$.

μ **values**	0.6	0.65	0.7	0.75	0.8	**WINS**
0.6	\	0	0	0	1	1
0.65	1	\	0	0	1	2
0.7	1	1	\	0	1	3
0.75	1	1	1	\	1	**4**
0.8	0	0	0	0	\	0
LOSSES	3	2	1	**0**	4	**10**

Table 5.4: Third round of the adaptive Round-Robin tournament, final version. Threshold of 0.05, centered on 0.7 and range of $[0.6, 0.8]$.

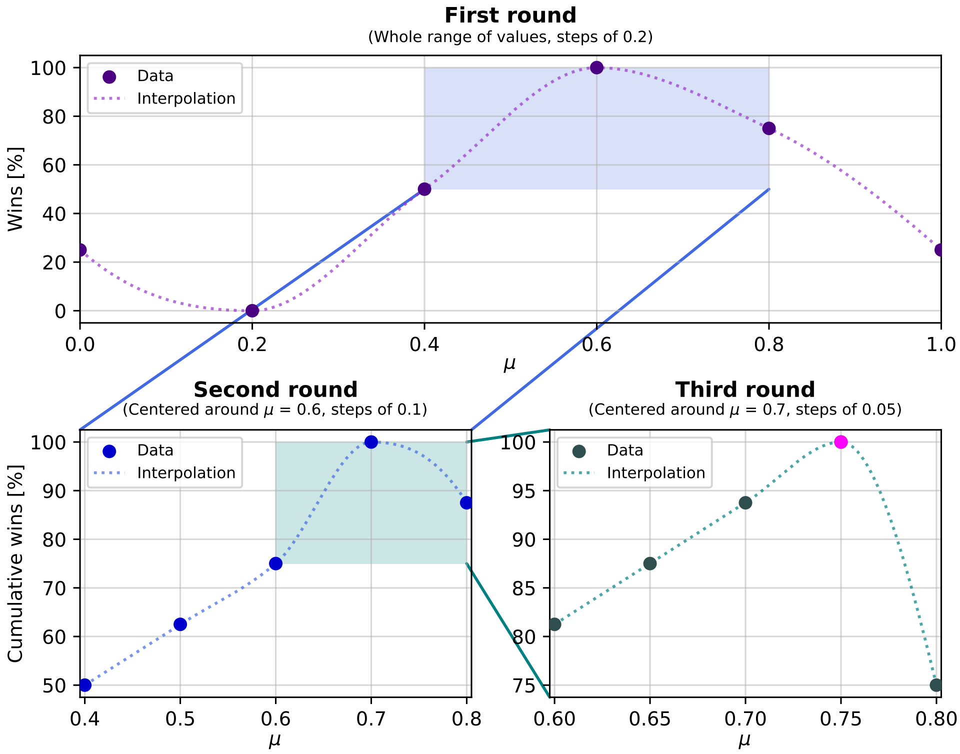

Figure 5.15: Psychophysical experiment carried out on the final primitives definition.

Discussion. The psychophysical experiments conducted allowed to assert the optimum values for the peak location parameter of the force profile. The peak width was also determined but by trials. The new definition of the primitives allowed to significantly increase the width from 0.2 to 0.5. The final value makes sense given that the subject should be assisted during the whole flexion phase of the gait cycle. Even though the flexion movement lasts less than the extension one, a small amount of residual assisting force before and after the flexion is not perceived by the wearer, hence a larger width than the actual movement.

As for the peak location, the results were overall the same with only a slightly earlier peak for the new value (0.8 before, and 0.75 for the final version). Since the flexion movement lasts less than half the phase, this means that the peak occurs at the beginning of the movement. An impulse at the start of the lifting process in indeed preferred since the hip velocity has to decrease at the end to prepare for the reverse motion.

The psychophysical test showed the sensibility of the parameters; a slight variation is perceived by the user. However, deciding between two values can be tricky and the choices are not always steady from one round to another. It would be interesting to redo the experiment for a larger group of subjects to draw more conclusions and maybe settle on a general optimum value.

5.3.2 Study of the optimum and maximum forces according to the velocity

Goal. The last parameter of interest is the amplitude factor A. As previously assessed, the speed has a major influence on the force required to assist the subject. This experiment studies the relationship between velocity and force amplitude.

Methods. Two values are determined for multiple walking speeds: the optimum assistance and the maximum one. They are both determined by progressively increasing the assistance level until the subject feels its assisted leg follows the walk without requiring any action from its part, and then a second level is asserted when the subject feels any more assistance could result in a knock-off. For the first level reached, the subject has to feel like its leg is passive and moves independently form its will (without refraining it though). And the second level is reached when the user needs to be holding onto the treadmill to keep its balance.

Seven different velocities were tested: 1.5 km/h, 2 km/h, 2.5 km/h, 3 km/h, 3.5 km/h, 4 km/h and 4.5 km/h. Even though an hemiparetic patient cannot walk that fast, the goal was to see the evolution of the force, and slower speeds (i.e., like for the patients) are not natural for the sound subject.

Results. The two curves representing the ideal and maximum force setpoints are plotted in Figure 5.16. The first observation concerns the optimum force profile which do not behave linearly with the speed. Indeed, the values for the slower speeds are more spaced that the ones for the faster speeds that do not change as much.

Regarding the maximum values, they seem to behave the opposite way with increasing steps along the speeds. However, due to the orthosis limit determined previously, the last three velocities could not be correctly assessed.

Remarks: the results plotted in the graph are the setpoints used in the mid-level controller but, as stated before, losses occur and the forces being really measured by the sensor are always slightly lower. Also, the setpoints are written as the norms of the force vectors; when considered with their direction, a minus sign should be added.

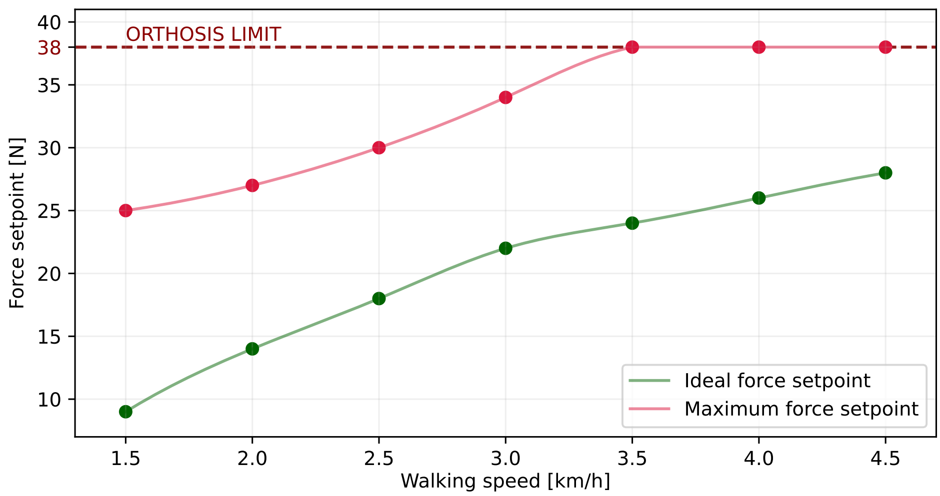

Figure 5.16: Optimum and maximum force setpoints with respect to the walking speed.

Discussion It is of great importance to assess the required assistive force regarding the speed and the intentions of the user. This experiment was conducted on a sound patient, the levels of forces determined by it should therefore be adjusted in the future for the needs of hemiparetic patients. It is however worth noticing that, even though the maximum force produced being measured by the sensor is slightly lower than the initial goal of the orthosis, the optimum levels of force are always far below this limit. One could wonder if the goal has been properly set and if it maybe needs to be adjusted to the device's performances. H.E.R.O. is able to sufficiently assist the wearer, even at high speeds. The device should therefore produce enough assistance for hemiparetic patients, especially at slow paces.

The force needs to be set properly as it has a major impact of the subject stride and an hemiparetic patient could easily lose its balance in case the assistance is set too high. Figure 5.17 illustrates the effect of excessive assistance for the stride length by comparing the normal stride of the subject with the stride obtained with a too powerful impulse from the device: the stride length increases by a few centimeters.

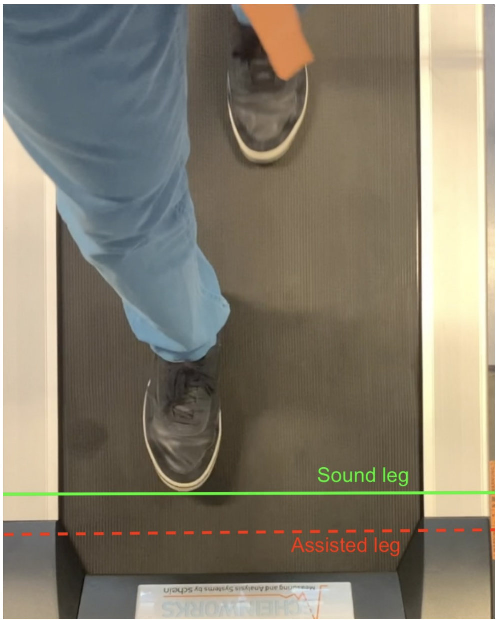

(a) Sound stride.

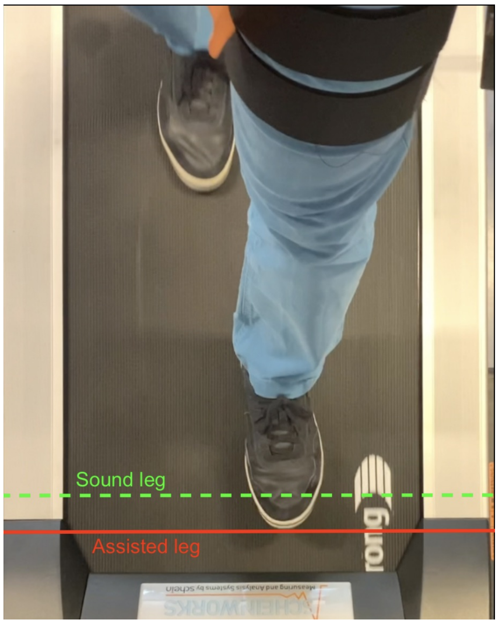

(b) Assisted stride.

Figure 5.17: Stride comparison between the assisted leg and the control one.

Chapter 6

Conclusion and future perspectives

The work accomplished during this master's thesis allowed to implement an effective assistance control to the H.E.R.O. hip orthosis. The user is now able to receive an adaptable assistance phase-synchronized with its gait without the past discomfort. The force delivered can be modulated by three parameters, the peak location, width and amplitude, to adjust the occurrence within a cycle and the assistance level. As for the performance goals set for this project, the current prototype is able to fulfill them. The ideal assistance value, established at 40% of the biological torque, is reached when the device is used at its maximum capacity; the lower bound, set to 20%, is achieved without any difficulties. The controller designed withstands changes in gait velocity almost instantaneously, except for some delays with respect to the halt detection.

A second focus of this work was about improving the prototype structure and electro-mechanical design with slight alterations to enhance the user's comfort and lighten the device, as well as address the electronics current saturation issues, notably with the use of the parallel spring. Improvements of the wiring system have also been carried out with a new design for the electronics support piece, the consolidation and clean up of the cables, and the creation of a file gathering all the information about the connections.

The performances of the current prototype have been investigated by conducting multiple experiments to assess its different functionalities. A psychophysical study has even been carried out in the process of determining the optimum controller's settings. They have however been executed on only one sound subject; experimental experiments on a larger group of subjects, including hemiparetic patients, might bring out other results and should therefore be conducted in the future. Nevertheless, these preliminary assessments showed that H.E.R.O. is able to dynamically assist a sound subject and that the level of assistance available exceeds its needs, even for fast paces. Moreover, the parallel spring can finally be integrated without causing any saturation issue for the device, and it offers a very valuable contribution to the assistance produced.

A list of future improvements about the orthosis' structure design has already been drawn up in Section 3.2. The most important ones are the design of a system addressing the movement obstruction brought by the spring, as well as a better cooling management for the motor. Along any structural changes, the weight optimization should also be taken into account.

Outside of the future enhancements regarding the device's structure, the next works should aim at finishing off the mid-level controller by addressing the remaining issues encountered with the current saturation in transparent mode, and the halt detection period. The future perspectives could also include a more thorough PID optimization as an attempt to reduce the gap between the setpoint and the force measured. The motor might need to be investigated regarding the steps generated when using the spring. Finally, a high-level controller needs to be implemented to enable the subject's intentions to be integrated in the device with the ultimate goal of providing adequate assistance for the user's mobility.

The current orthosis prototype constitutes a strong basis for the development of a final, wearable and adequate device. The H.E.R.O. is born.

Appendix A

LabVIEW programs

Figure A.1 shows a simplified representation of the LabVIEW implementation structure. Three main blocks are highlighted as they are the only ones being explained in this work. The mid-level controller being already study in depth in Section 4.2, only the two other blocks are further detailed here.

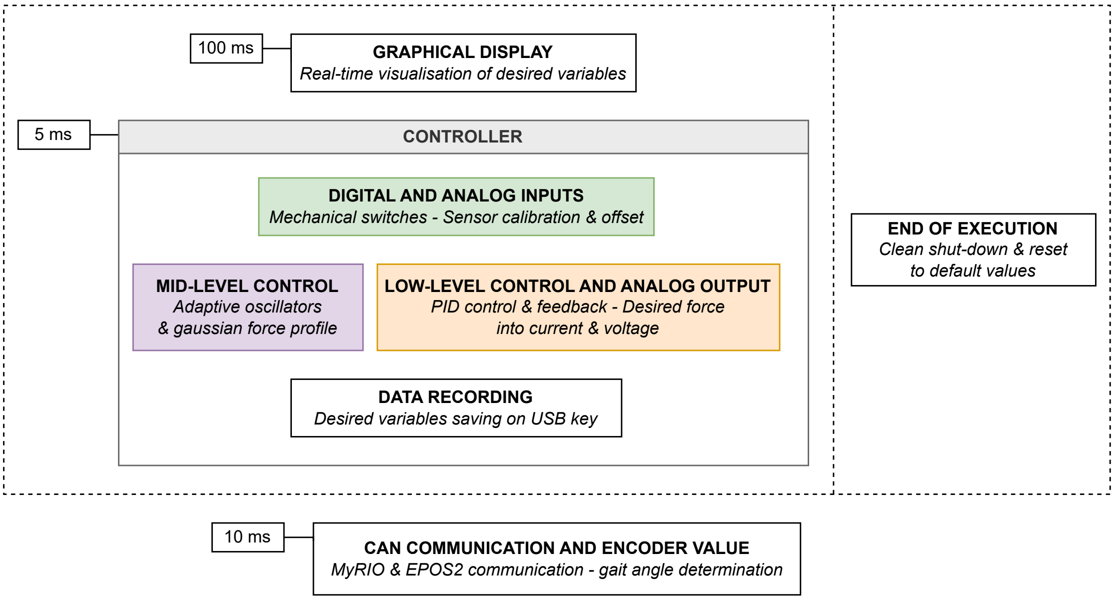

Figure A.1: LabVIEW general architecture

The first block being zoomed in is the block relative to the analog and digital inputs from the sensor and the mechanical switch respectively. The corresponding block diagram is shown in Figure A.2.

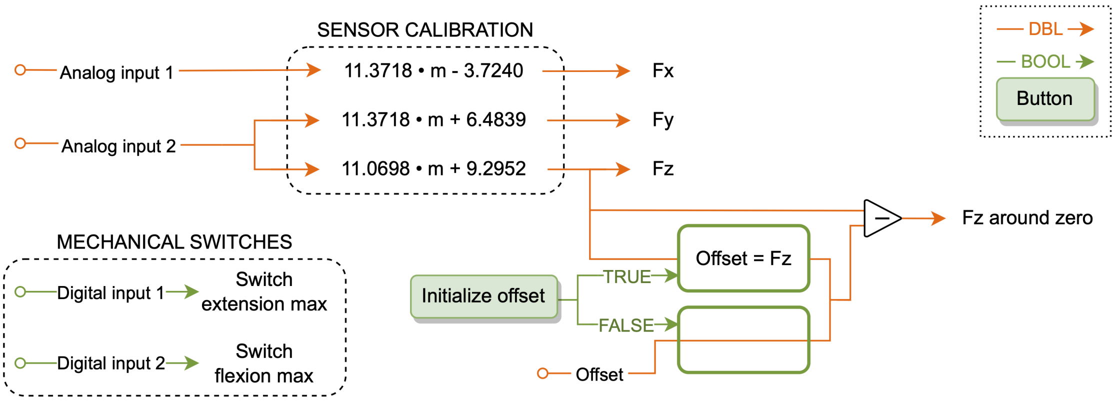

Figure A.2: Analog and digital inputs block diagram

The second block detailed is the one about the mid-level control and analog output. As a reminder, a general overview of the low-level controller has been described in Section 3.1.2. However, Figure A.3 gives a more complete diagram of the block.

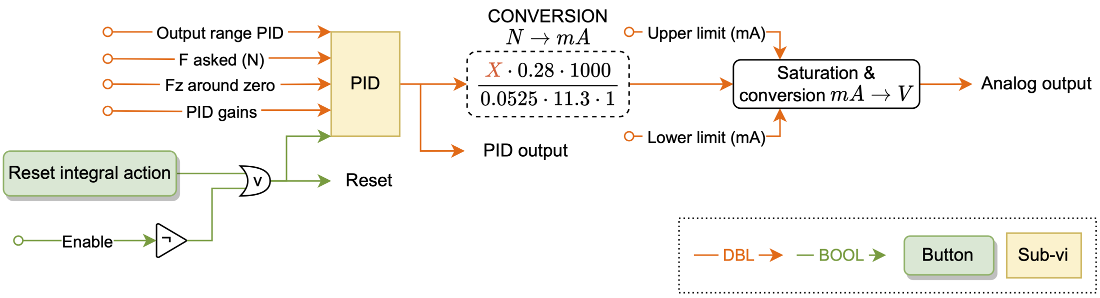

Figure A.3: Low-level controller block diagram

Appendix B

Components specifications

The hardware used for the orthosis is composed of an EC motor with a built-in encoder, a driver, a force sensor and a myRIO device. Here are their references and the datasheets for the motor, its encoder and the driver (see next pages) [34].

- The motor used is the EC60flat, brushless, 150W motor from Maxon Motor. It has an integrated encoder of 1024ppr. The serial number of the motor alone is 647694 and the combination with the encoder is 662151.
- The driver is the EPOS2 70/10 from Maxon Motor, its reference number is 375711.
- The sensor is a 6 axis force sensor (force: ± 15 lb; torque: ± 50 lb). Its reference is FT3025, 15/50 from Assurance Technologies Inc.
- The NI myRIO-1900 is a portable reconfigurable I/O device from National Instruments.

The orthosis can me mounted with a parallel spring of resting length $l_0 = 0.15[m]$ and rigidity constant $k_p = 1.4[\frac{N}{mm}]$. Its serial number is AWS18-150 from Misumi.

A second spring is available but unused at the moment as it is too rigid for the current prototype. Its resting length is $l_0 = 0.15[m]$ and its rigidity constant is $k_p = 3.92[\frac{N}{mm}]$. Its serial number is AWT16-150 from Misumi.

EC 60 flat ∅60 mm, brushless, 150 watt

Open Rotor

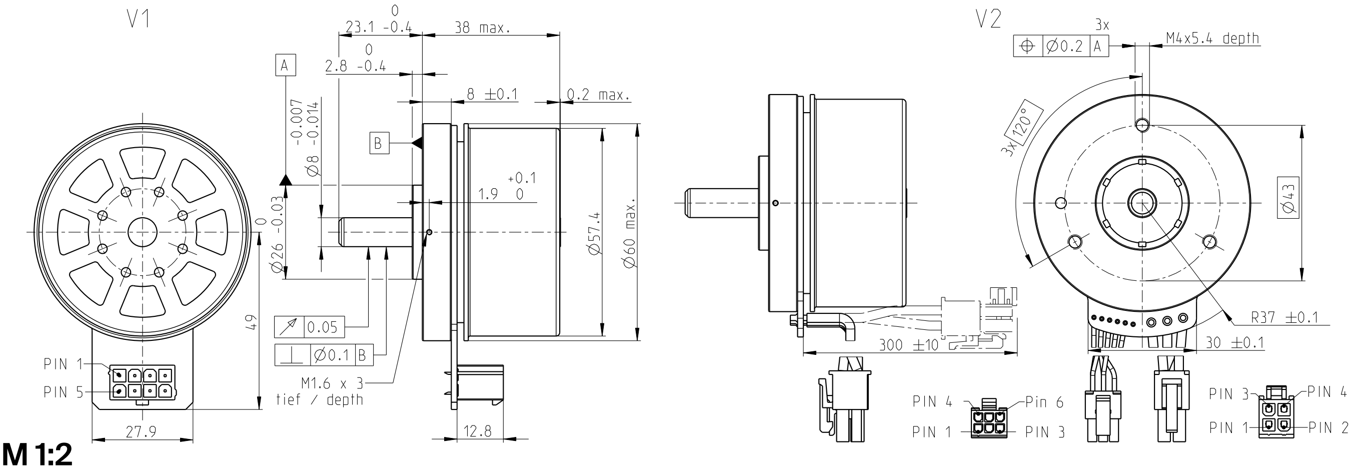

M 1:2

Stock program	
Standard program	
Special program (on request)	

Part Numbers

V1 with Hall sensors	625857	625858	625859
V2 with Hall sensors and cables	647693	647694	647695

Motor Data

	Values at nominal voltage				
1	Nominal voltage	V	12	24	48
2	No load speed	rpm	3760	4300	4020
3	No load current	mA	815	497	224
4	Nominal speed	rpm	2990	3480	3230
5	Nominal torque (max. continuous torque)	mNm	378	401	437
6	Nominal current (max. continuous current)	A	12*	7.25	3.63
7	Stall torque[1]	mNm	3340	4300	4870
8	Stall current	A	111	81.9	43.2
9	Max. efficiency	%	83.8	85.2	86.3
	Characteristics				
10	Terminal resistance phase to phase	Ω	0.108	0.293	1.11
11	Terminal inductance phase to phase	mH	0.0911	0.279	1.28
12	Torque constant	mNm/A	30	52.5	113
13	Speed constant	rpm/V	318	182	84.8
14	Speed/torque gradient	rpm/mNm	1.14	1.01	0.837
15	Mechanical time constant	ms	9.68	8.6	9.1
16	Rotor inertia	gcm²	810	810	810

Specifications

Thermal data

17	Thermal resistance housing-ambient	1.94 K/W
18	Thermal resistance winding-housing	1.48 K/W
19	Thermal time constant winding	16.1 s
20	Thermal time constant motor	69.9 s
21	Ambient temperature	-40...+100°C
22	Max. winding temperature	+125°C

Mechanical data (preloaded ball bearings)

23	Max. speed	6000 rpm
24	Axial play at axial load < 12.0 N	0 mm
	> 12.0 N	0.14 mm
25	Radial play	preloaded
26	Max. axial load (dynamic)	12 N
27	Max. force for press fits (static)	170 N
	(static, shaft supported)	8000 N
28	Max. radial load, 5 mm from flange	112 N

Other specifications

29	Number of pole pairs	7
30	Number of phases	3
31	Weight of motor	350 g

Values listed in the table are nominal.

Connection V1		**V2** (sensors, AWG 24)
Pin 1	Hall sensor1	Hall sensor1
Pin 2	Hall sensor 2	Hall sensor 2
Pin 3	V_{Hall} 4.5...24 VDC	Hall sensor 3
Pin 4	Motor winding 3	GND
Pin 5	Hall sensor 3	V_{Hall} 4.5...24 VDC
Pin 6	GND	N.C.
Pin 7	Motor winding 1	
Pin 8	Motor winding 2	

	V2 (Motor, AWG 16)
Pin 1	Motor winding 1
Pin 2	Motor winding 2
Pin 3	Motor winding 3
Pin 4	N.C.

Wiring diagram for Hall sensors see p. 59

Connector		**Part number**
Molex	46015-0806	43025-0600
Molex		39-01-2040

Connection cable for V1

Universal, L = 500 mm	**339380**
to EPOS4, L = 500 mm	**354045**

[1]Calculation does not include saturation effect (p. 71/178)

Operating Range

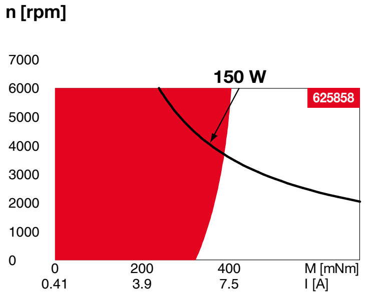

Comments

Continuous operation
In observation of above listed thermal resistance (lines 17 and 18) the maximum permissible winding temperature will be reached during continuous operation at 25°C ambient.
= Thermal limit.

Short term operation
The motor may be briefly overloaded (recurring).

Assigned power rating

maxon Modular System Details on catalog page 46

Planetary Gearhead
∅52 mm
4-30 Nm
Page 411

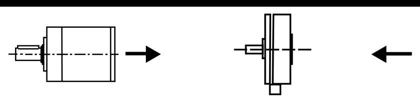

Encoder MILE
512-4096 CPT,
2 channels
Page 462

Recommended Electronics:

Notes	**Page 46**
ESCON Module 50/5	501
ESCON Mod. 50/8 (HE)	502
ESCON 50/5	503
ESCON 70/10	503
DEC Module 50/5	505
EPOS4 Mod./Comp. 50/5	510
EPOS4 Mod./Comp. 50/8	511
EPOS4 Mod./Comp. 50/15	514
EPOS4 50/5	515
EPOS4 70/15	515
EPOS4 Disk 60/8	516
EPOS4 Disk 60/12	517
EPOS2 P 24/5	520

*In combination with EPOS4 positioning controllers, the connector technology limits the nominal current (max. continuous current load) is limited to 11 A.

mdp

Moteur Brushless EC60flat 150W/MILE

Les avantages :
Codeur intégré 1024pts
Forme plate adaptées aux espaces limités
Rotor externe ouvert pour plus de puissance

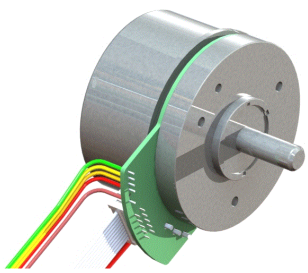

Les produits associés :

> Alimentation
DRP-240-24
DRP-480S-24
RS-100-24
RS-150-24
SP-320-24
> Cartes électroniques
EPOS2P 24/5
EPOS4 50/5
EPOS4 70/15
ESCON 50/5
ESCON 70/10

maxon motor — 146 W - 252 W

Tension d'alimentation (Ua)	V	24
Vitesse au courant In	tr/mn	3480
Couple au courant In	mNm	401.00
Courant maximum permanent In	mA	7250
Vitesse à vide à Ua à +/- 10%	tr/mn	4300
Courant à vide à +/- 50%	mA	497
Courant de démarrage à Ua	mA	81900
Couple de démarrage à Ua	mNm	4 300.00
Constante de couple	mNm/A	52.50
Constante de vitesse	tr/mn/V	182
Pente vitesse/couple	tr/mn/mN	1
Vitesse limite	tr/mn	6000
Puissance utile maximum à Ua	W	485
Rendement maximum	%	85.2
Constante de temps	ms	8.6
Inertie	gcm²	810
Résistance aux bornes	Ohm	0.293
Inductance	mH	0.279
Résistance thermique	K/W	1.94
Résistance thermique	K/W	1.48
Cste Tps thermique Bobinage	s	16.1
Cste Tps thermique Boîtier	s	69.9
Tension de mesure	V	24
Puissance utile nominale	W	146
Puissance utile max permanente	W	252

Commutation	électronique
Nombre de phases	3
Paliers	Roulements à billes
Charge axiale maximum (dynamique)	12 N
Jeu axial minimum	0 mm
Jeu axial maximum	0.14 mm
Charge radiale maximum	112 N
à une distance de la face de :	5 mm
Jeu radial	précontraint mm
Force de chassage maximum (statique)	170 N
Si axe arrière tenu	8000 N
Température ambiante minimum de	-40 °C
Température ambiante maximum de	+100 °C
Température maximum du bobinage	+125 °C
Poids	350 g

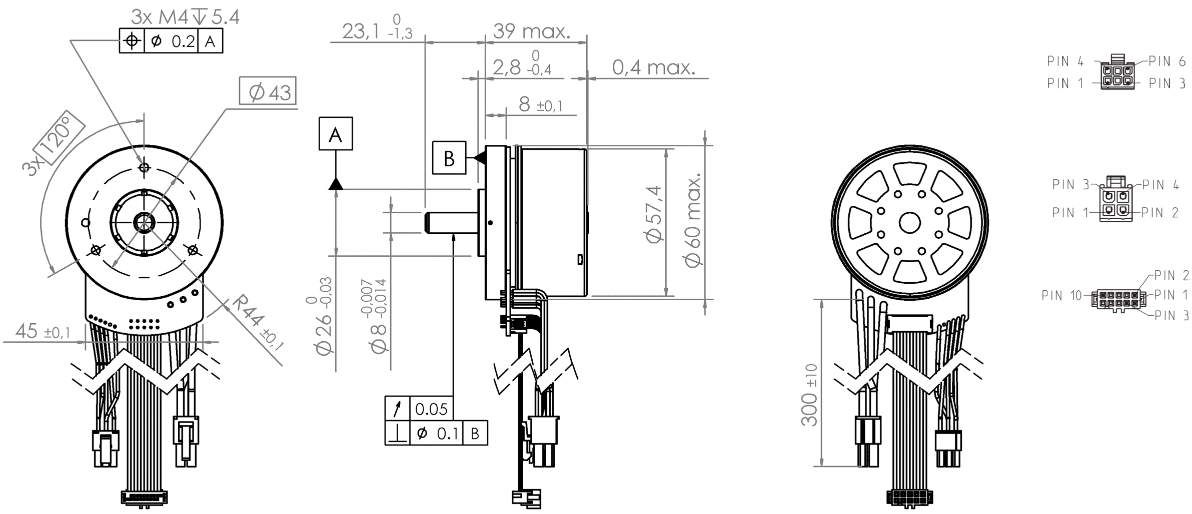

Sensors (AWG 24)
Pin 1 Hall sensor 1
Pin 2 Hall sensor 2
Pin 3 Hall sensor 3
Pin 4 GND
Pin 5 V_{Hall} 4.5...18 VDC
Pin 6 N.C.
Motor (AWG 16)
Pin 1 Motor winding 1
Pin 2 Motor winding 2
Pin 3 Motor winding 3
Pin 4 Not connected
Encoder (AWG 28)
Pin 1 N.C.
Pin 2 V_{CC}
Pin 3 GND
Pin 4 N.C.
Pin 5 Channel $\overline{A}$
Pin 6 Channel A
Pin 7 Channel $\overline{B}$
Pin 8 Channel B
Pin 9 Do not connect
Pin 10 Do not connect

43025-600 Molex
39-01-2040 Molex
DIN 41651/EN 60603-13

Editionfévrier 2021 / sous réserve de modifications

EPOS2 24/5
Matched with DC brush motors with encoder or brushless EC motors with Hall sensors and encoder to 120/240 watts.

EPOS2 50/5
Matched with DC brush motors with encoder or brushless EC motors with Hall sensors and encoder to 250/500 watts.

EPOS2 70/10
Matched with DC brush motors with encoder or brushless EC motors with Hall sensors or encoder to 700/1750 watts.

Controller versions		
CANopen Slave	**CANopen Slave**	**CANopen Slave**
Electrical data		
11 - 24 VDC	11 - 50 VDC	11 - 70 VDC
11 - 24 VDC	11 - 50 VDC	11 - 70 VDC
0.9 x V_{CC}	0.9 x V_{CC}	0.9 x V_{CC}
10 A	10 A	25 A
5 A	5 A	10 A
50 kHz	50 kHz	50 kHz
10 kHz	10 kHz	10 kHz
1 kHz	1 kHz	1 kHz
1 kHz	1 kHz	1 kHz
25 000 rpm (sinusoidal); 100 000 rpm (block)	25 000 rpm (sinusoidal); 100 000 rpm (block)	25 000 rpm (sinusoidal); 100 000 rpm (block)
15 µH / 5 A	22 µH / 5 A	25 µH / 10 A
Input		
H1, H2, H3	H1, H2, H3	H1, H2, H3
A, A\, B, B\, I, I\ (max. 5 MHz)	A, A\, B, B\, I, I\ (max. 5 MHz)	A, A\, B, B\, I, I\ (max. 5 MHz)
6 (TTL and PLC level)	11 (7 optically isolated, 4 differential)	10 (7 optically isolated, 3 differential)
2 (12-bit resolution, 0…+5 V)	2 (differential, 12-bit resolution, ±10 V)	2 (differential, 12-bit resolution, 0…+5 V)
configurable with DIP switch 1…7	configurable with DIP switch 1…7	configurable with DIP switch 1…7
Output		
4	5 (4 optically isolated, 1 differential)	5 (4 optically isolated, 1 differential)
	1 (12-bit, 0…10 V, max. 1 mA)	
+5 VDC, max 100 mA	+5 VDC, max. 100 mA	+5 VDC, max. 100 mA
+5 VDC, max. 30 mA	+5 VDC, max. 30 mA	+5 VDC, max. 30 mA
V_{CC}, max. 1300 mA	+5 VDC, max. 150 mA	+5 VDC, max. 150 mA; +5 VDC (R_i = 1 kΩ)
Interface		
RxD; TxD (max. 115 200 bit/s)	RxD; TxD (max. 115 200 bit/s)	RxD; TxD (max. 115 200 bit/s)
high; low (max. 1 Mbit/s)	high; low (max. 1 Mbit/s)	high; low (max. 1 Mbit/s)
Data+; Data- (max. 12 Mbit/s)	Data+; Data- (max. 12 Mbit/s)	Data+; Data- (max.12 Mbit/s)
Indicator		
green LED, red LED	green LED, red LED	green LED, red LED
Environmental conditions		
-10…+55°C	-10…+45°C	-10…+45°C
+55…+83°C; Derating: -0.179 A/°C	+45…+80°C; Derating: -0.143 A/°C	+45…+85°C; Derating: -0.250 A/°C
-40…+85°C	-40…+85°C	-40…+85°C
5…90%	5…90%	5…90%
Mechanical data		
Approx. 170 g	Approx. 240 g	Approx. 330 g
105 x 83 x 24 mm	120 x 93.5 x 27 mm	150 x 93 x 27 mm
Flange for M3-screws	Flange for M3-screws	Flange for M3-screws
Part numbers		
367676 EPOS2 24/5	**347717** EPOS2 50/5	**375711** EPOS2 70/10
Accessories		
309687 DSR 50/5 Shunt regulator	**309687** DSR 50/5 Shunt regulator	**235811** DSR 70/30 Shunt regulator
Order accessories separately, see page 470	Order accessories separately, see page 470	Order accessories separately, see page 470

Appendix C

CAD models

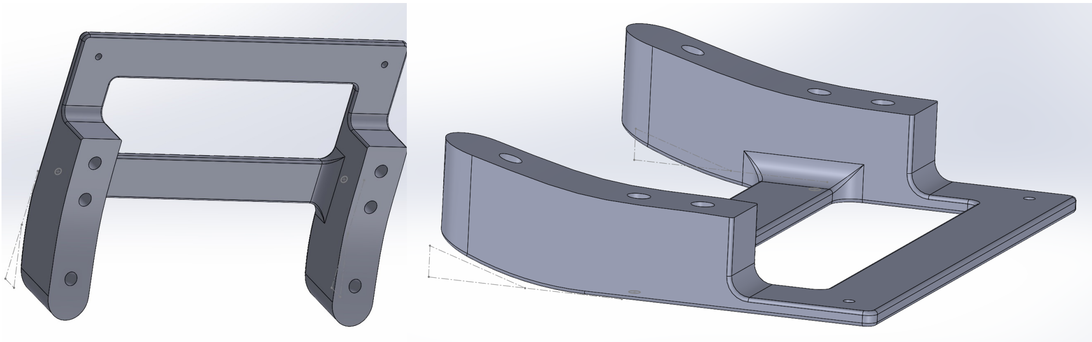

Figure C.1: Electronics support: plain views.

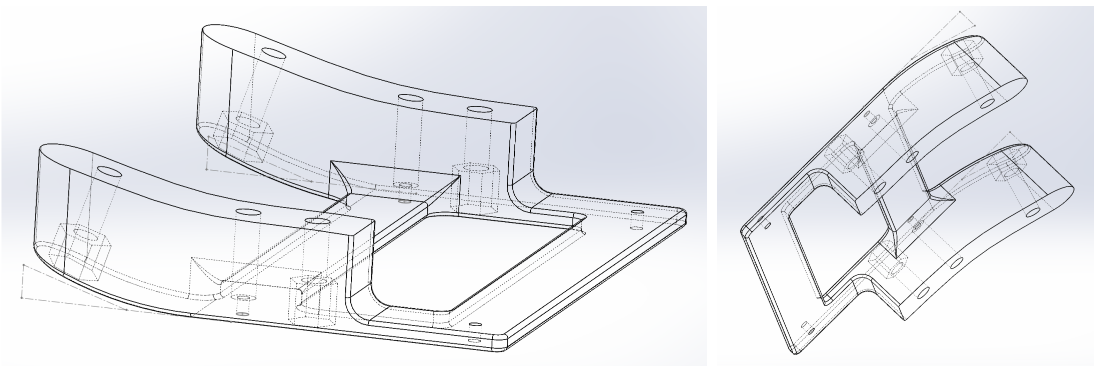

Figure C.2: Electronics support: transparent views.

Appendix D

Additional figures

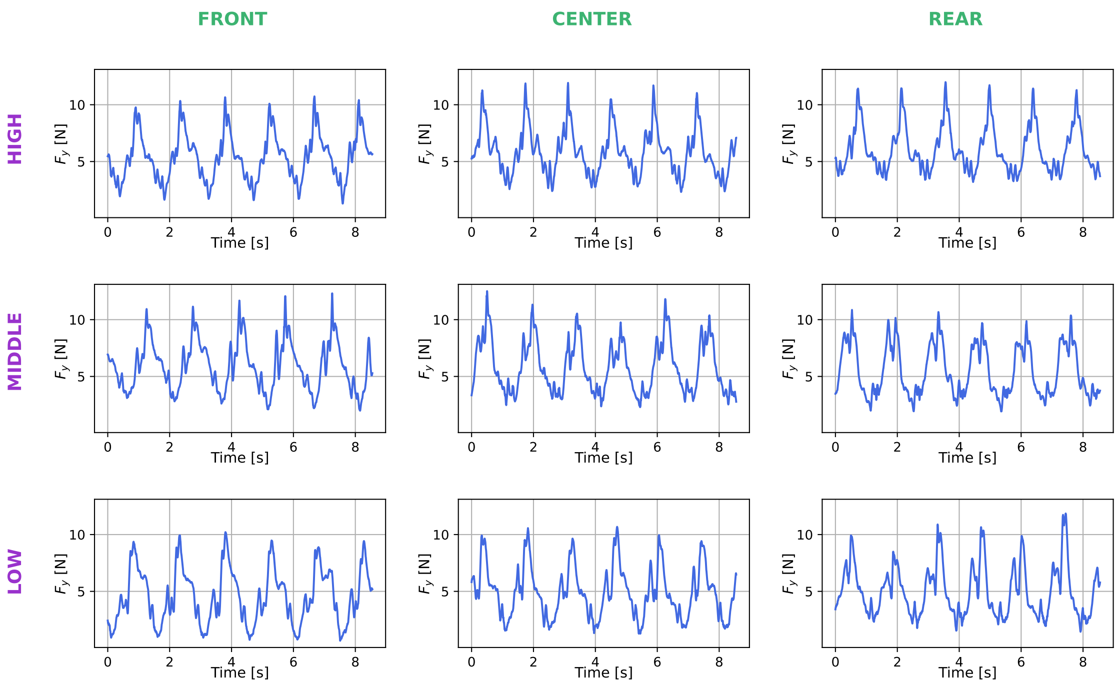

Figure D.1: Frontal forces measured by the sensor while in transparent mode, at 3 km/h. Multiple configurations of the corset are displayed. In green: the horizontal displacements; in purple: the vertical ones.

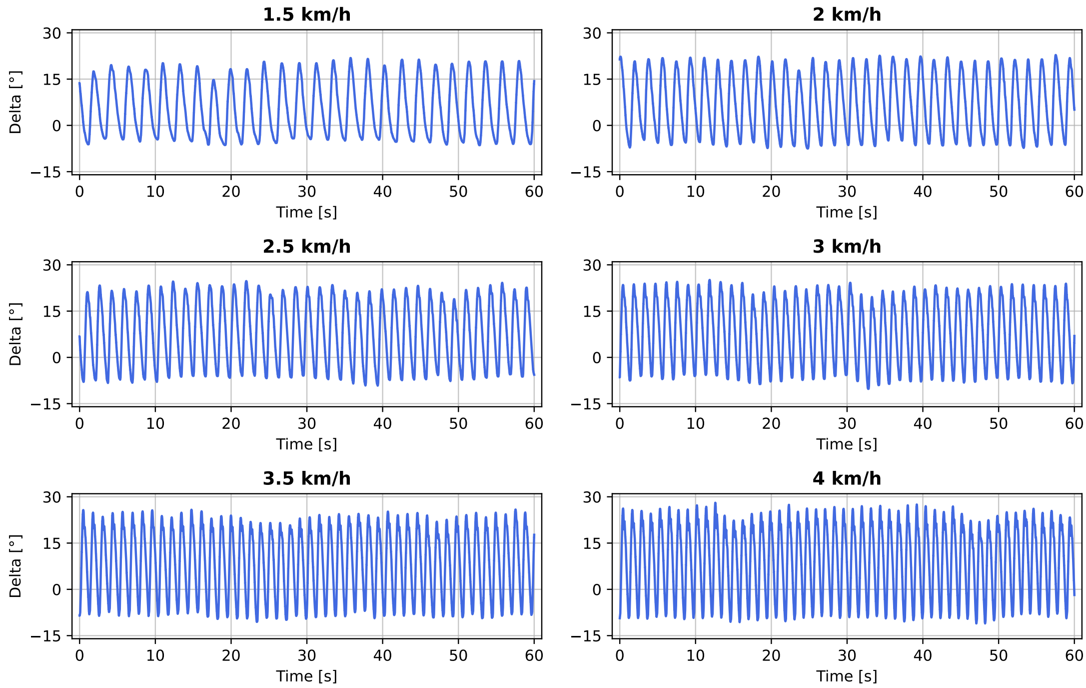

Figure D.2: Hip angular position, reference plots for various speeds in transparent mode without the parallel spring.

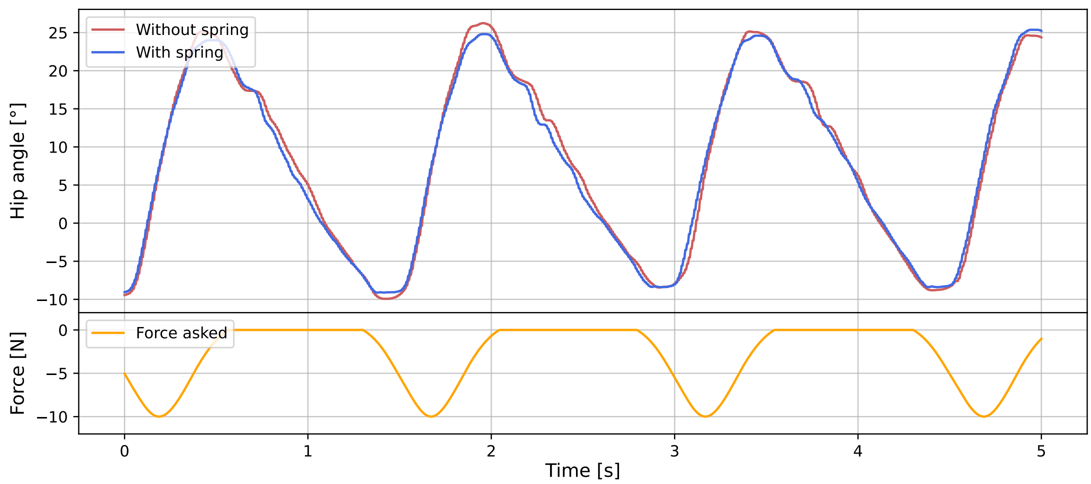

Figure D.3: Hip angular position, with and without spring, at a speed of 2.5 km/h. Assistance of -10 N.

μ values	0.2	0.4	0.6	0.8	1.0	**WINS**
0.2	\	0	0	0	0	0
0.4	1	\	0	0	0	1
0.6	1	1	\	0	1	3
0.8	1	1	1	\	1	**4**
1.0	1	1	0	0	\	2
LOSSES	4	3	1	**0**	2	**10**

Table D.1: First round of the adaptive Round-Robin tournament, initial version. Threshold of 0.2 and range of $]0, 1.0]$.

μ values	0.6	0.7	0.8	0.9	1.0	**WINS**
0.6	\	0	0	0	1	1
0.7	1	\	0	0	1	2
0.8	1	1	\	1	1	**4**
0.9	1	1	0	\	1	3
1.0	0	0	0	0	\	0
LOSSES	3	2	**0**	1	4	**10**

Table D.2: Second round of the adaptive Round-Robin tournament, initial version. Threshold of 0.1, centered on 0.8 and range of $[0.6, 1.0]$.

μ values	0.7	0.75	0.8	0.85	0.9	**WINS**
0.7	\	0	0	0	0	0
0.75	1	\	0	0	1	2
0.8	1	1	\	1	1	**4**
0.85	1	1	0	\	1	3
0.9	1	0	0	0	\	1
LOSSES	4	2	**0**	1	3	**10**

Table D.3: Third round of the adaptive Round-Robin tournament, initial version. Threshold of 0.05, centered on 0.8 and range of $[0.7, 0.9]$.

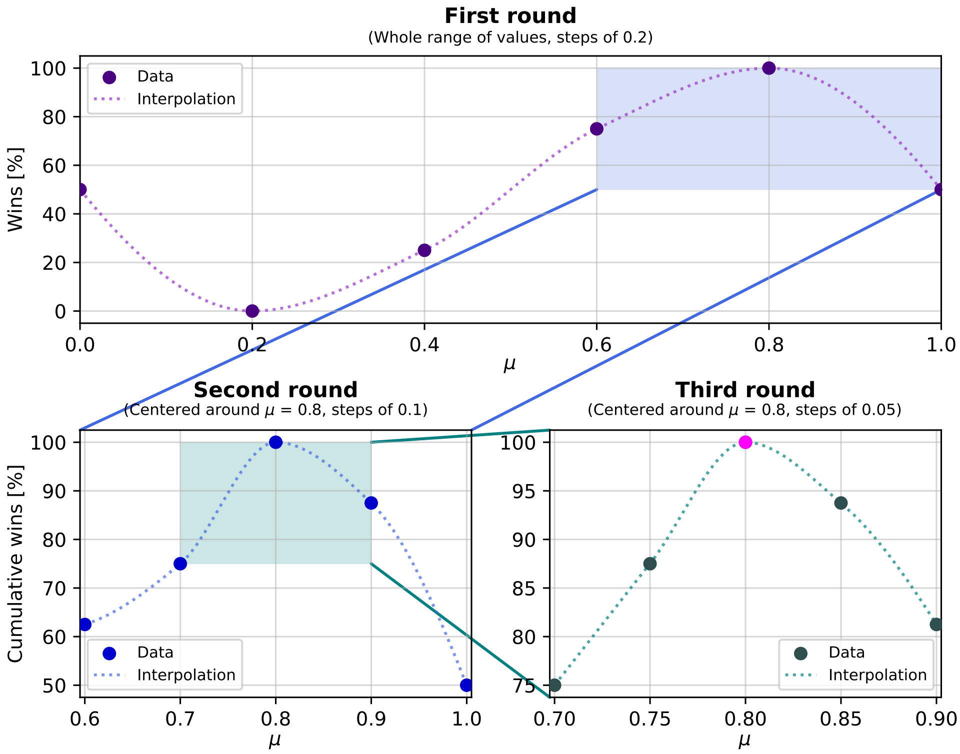

Figure D.4: Psychophysical experiment carried out on the initial primitives definition.

Bibliography

[1] K. Budig and E. Harding, editors. *Secondary prevention of heart attack and stroke: country profile for Belgium*. The Health Policy Partnership, London, 2021.

[2] World Health Organization. The top 10 causes of death. https://www.who.int/news-room/fact-sheets/detail/the-top-10-causes-of-death. [Accessed: 2023-08-10].

[3] L.R. Sheffler and J. Chae. Hemiparetic gait. *Phys Med Rehabil Clin N Am*, 26:611–623, 2015.

[4] R. Wilson and P. Raghavan, editors. *Stroke Rehabilitation*. Elsevier, 2019.

[5] M.N. Bartels, C.A. Duffy, and H.E. Beland. *Pathophysiology, medical management, and acute rehabilitation of stroke survivors*, pages 2–45. Elsevier, 2015.

[6] N.R. Dhiman, G.L. Shah, D. Joshi, and V. Gyanpuri. Relationship between side of hemiparesis and functional independence using activities of daily living index. *Journal of the Anatomical Society of India*, 63:S30–S35, 2014.

[7] J.B. Webster and D.P. Murphy, editors. *Atlas of Orthoses and Assistive Devices (Fifth Edition)*. Elsevier, Philadelphia, 2019.

[8] Human Technology Inc. What's the difference between orthotics and prosthetics. https://humantechpando.com/whats-the-difference-between-orthotics-and-prosthetics/. [Accessed: 2023-08-10].

[9] M. Guillaumie and N. Lejeune. Design and experimental performance assessment of a hip flexion assistive device. Master's thesis, Louvain School of Engineering (EPL), UCLouvain, 2018.

[10] C. Pestiaux. Conception, command and experimental validation of a hip flexion assistive device. Master's thesis, Louvain School of Engineering (EPL), UCLouvain, 2019.

[11] J. Desbrosses. Rehab robotics - design and experimental performance assessment of a hip flexion assistive device. Master's thesis, Louvain School of Engineering (EPL), UCLouvain, 2021.

[12] N. Sturam. Rehab robotics - design and experimental performance assessment of a hip flexion assistive device. Master's thesis, Louvain School of Engineering (EPL), UCLouvain, 2022.

[13] X. Zhang. *Computational Modelling of Biomechanics and Biotribology in the Musculoskeletal System (Second Edition)*. Woodhead Publishing, 2021.

[14] Chegg. Body axes. https://www.chegg.com/learn/topic/body-axes. [Accessed: 2023-07-23].

[15] M.W. Whittle. *Gait Analysis (Fourth Edition)*. Butterworth-Heinemann, Edinburgh, 2007.

[16] J. Moore, S. Hnat, and A. van den Bogert. An elaborate data set on human gait and the effect of mechanical perturbations. *PeerJ*, 3:e918, 2015.

[17] Cleveland Clinic. Hemiparesis. https://my.clevelandclinic.org/health/symptoms/24952-hemiparesis. [Accessed: 2023-07-24].

[18] K. Honda, Y. Sekiguchi, T. Muraki, and S.-I. Izumi. The differences in sagittal plane whole-body angular momentum during gait between patients with hemiparesis and healthy people. *Journal of Biomechanics*, 86:204–209, 2019.

[19] M.R. Tucker, J. Olivier, A. Pagel, H. Bleuler, M. Bouri, O. Lambercy, J.D.R. Millán, R. Riener, H. Vallery, and R. Gassert. Control strategies for active lower extremity prosthetics and orthotics: a review. *Journal of NeuroEngineering and Rehabilitation*, 12, 2015.

[20] Maziar A. Sharbafi and André Seyfarth, editors. *Bioinspired Legged Locomotion*. Butterworth-Heinemann, 2017.

[21] J. González-Vargas, J. Ibáñez, J.L. Contreras-Vidal, H. van der Kooij, and J.L. Pons, editors. *Wearable Robotics: Challenges and Trends*. Springer International Publishing, Cham, 2016.

[22] A. Accogli, L. Grazi, S. Crea, A. Panarese, J. Carpaneto, N. Vitiello, and S. Micera. Emg-based detection of user's intentions for human-machine shared control of an assistive upper-limb exoskeleton. In *Wearable Robotics: Challenges and Trends*, pages 181–185, Cham, 2017. Springer International Publishing.

[23] Carnegie Mellon University. Robo-ankle. https://www.cmu.edu/homepage/health/2014/winter/robotic-orthotic.shtml. [Accessed: 2023-07-25].

[24] B. Chen, H. Ma, L.-Y. Qin, F. Gao, K.-M. Chan, S.-W. Law, L. Qin, and W.-H. Liao. Recent developments and challenges of lower extremity exoskeletons. *Journal of Orthopaedic Translation*, 5:26–37, 2016. Special Issue: Orthopaedic Biomaterials and Devices.

[25] K. Lee, D. Liu, L. Perroud, R. Chavarriaga, and J.D.R. Millán. Endogenous control of powered lower-limb exoskeleton. In *Wearable Robotics: Challenges and Trends*, pages 115–119, Cham, 2017. Springer International Publishing.

[26] Rex Bionics. Reimaging rehabilitation. https://www.rexbionics.com. [Accessed: 2023-07-26].

[27] A.J. Young and D.P. Ferris. State of the art and future directions for lower limb robotic exoskeletons. *IEEE Trans Neural Syst Rehabil Eng*, 25:171–182, 2017.

[28] S. Qiu, W. Guo, F. Zha, J. Deng, and X. Wang. Exoskeleton active walking assistance control framework based on frequency adaptive dynamics movement primitives. *Front. Neurorobot*, 15, 2021.

[29] L. Righetti, J. Buchli, and A. Ijspeert. Dynamic hebbian learning in adaptive frequency oscillators. *Phys. D Nonlin. Phenom*, 216:269–281, 2006.

[30] R. Ronsse, T. Lenzi, N. Vitiello, B. Koopman, E. van Asseldonk, S.M.M. De Rossi, J. van den Kieboom, H. van der Kooij, M.C. Carrozza, and A. Jan Ijspeert. Oscillator-based assistance of cyclical movements: model-based and model-free approaches. *Med Biol Eng Comput*, 49:1173–1185, 2011.

[31] M.G. Bernal-Torres, H.I. Medellín-Castillo, and J.C. Arellano-González. Design and control of a new biomimetic transfemoral knee prosthesis using an echo-control scheme. *Journal of Healthcare Engineering*, 2018.

[32] T. Bacek, M. Moltedo, J. Gonzalez-Vargas, G.A. Prieto, M.C. Sanchez-Villamañan, J.C. Moreno, and D. Lefeber. The new generation of compliant actuators for use in controllable bio-inspired wearable robots. In *Wearable Robotics: Challenges and Trends*, pages 255–259, Cham, 2017. Springer International Publishing.

[33] S. Phelps. Four-bar mechanisms - GeoGebra. https://www.geogebra.org/m/xmAST89t. [Accessed: 2023-07-29].

[34] Maxon Motor. EC 60 flat, diameter 60 mm, brushless, 150 W, with Hall sensors and cables: catalog page.

[35] H. Laloyaux, C. Livolsi, A. Pergolini, S. Crea, N. Vitiello, and R. Ronsse. Simplified motor primitives for gait symmetrization: Pilot study with an active hip orthosis. *2023 IEEE International Conference on Robotics and Automation (ICRA)*, pages 10436–10442, 2023.

[36] R. Ronsse, S.M.M. De Rossi, N. Vitiello, T. Lenzi, M.C. Carrozza, and A. Jan Ijspeert. Real-time estimate of velocity and acceleration of quasi-periodic signals using adaptive oscillators. *IEEE Transactions on Robotics*, 29:783–791, 2013.

[37] T. Yan, A. Parri, V. Ruiz Garate, M. Cempini, R. Ronsse, and N. Vitiello. An oscillator-based smooth real-time estimate of gait phase for wearable robotics. *Auton Robot*, 41:759–774, 2017.

[38] H. Laloyaux and R. Ronsse. Extraction of simple monophasic motor primitives towards bio-inspired locomotion assistance. *2019 IEEE International Conference on Cyborg and Bionic Systems (CBS)*, pages 253–260, 2019.

[39] J. Wagenbach. Meaning and impact of "cogging torque" and "ripple torque" - Maxon. https://support.maxongroup.com/hc/en-us/articles/6726327972252-Meaning-and-impact-of-Cogging-torque-and-Ripple-torque-. [Accessed: 2023-08-03].

[40] F. Gabbiani and S.J. Cox. Chapter 28 - relating neuronal responses and psychophysics. *Mathematics for Neuroscientists (Second Edition)*, pages 463–473, 2017.

[41] A.M. Amlani and E.C. Schafer. Application of paired-comparison methods to hearing aids. *Trends in Amplification*, 13(4):241–259, 2009.

[42] A. Faridi Esfanjnai and M. Mohebbi. A signal detection reminder methodology to evaluate effects of odor–taste-taste interactions to enhance the perceived saltiness. *Food Research International*, 165:112464, 2023.

UNIVERSITÉ CATHOLIQUE DE LOUVAIN
École polytechnique de Louvain
Rue Archimède, 1 bte L6.11.01, 1348 Louvain-la-Neuve, Belgique | **www.uclouvain.be/epl**